THE JOURNAL OF COMPARATIVE NEUROLOGY 289:315–336 (1989)

Arborisation Pattern and Postsynaptic Targets of Physiologically Identified Thalamocortical Afferents in Striate Cortex of the Macaque Monkey

T.F. FREUND, K.A.C. MARTIN, I. SOLTESZ, P. SOMOGYI, AND D. WHITTERIDGE
Medical Research Council, Anatomical Neuropharmacology Unit, Department of Pharmacology, Oxford, OX1 3QT, England (T.F.F., K.A.C.M., I.S., P.S., D.W.); 1st Department of Anatomy, Semmelweis University Medical School, Budapest, H-1450 Hungary (T.F.F., I.S., P.S.)

ABSTRACT

The monosynaptic targets of different functional types of geniculocortical axons were compared in the primary visual cortex of monkeys. Single thalamocortical axons were recorded extracellularly in the white matter by using horseradish-peroxidase-filled pipettes. Their receptive fields were mapped and classified as corresponding to those of parvi- or magnocellular neurons in the lateral geniculate nucleus. The axons were then impaled and injected intraaxonally with horseradish peroxidase. Two magnocellular (MA) and two parvicellular (PA) axons were successfully recovered and reconstructed in three dimensions. The two MA axons arborised mainly in layer 4Cα, as did the two PA axons in layer 4Cβ. Few collaterals formed varicosities in layer 6. Both MA axons had two large, elongated clumps of bouton (approx. 300–500 × 600–1,200 μm each) and a small clump. One PA axon had two clumps (each with a core appr. 200 μm in diameter); the other had only one (appr. 150–200 μm in diameter). The PA axon with two clumps had 1,520 boutons; the other PA axon had 1,380; one MA axon had 3,200 boutons; and those of the more extensive MA axon were not counted. The distribution of postsynaptic targets as well as the number of synapses per bouton has been established for a sample of 150 PA boutons and 173 MA boutons from serial ultrathin sections. The MA axons made on average 2.1 synapses per bouton compared to 1.79 for one PA axon and 2.6 for the other. The sample of boutons taken from the two physiological types of axons contacted similar proportions of dendritic spines (52–68%), shafts (33–47%), and somata (0–3%). The postsynaptic elements were further characterized by immunostaining for GABA. All postsynaptic perikarya and some of the dendrites (4.5–9.5% of all targets) were positive for the amino acid. Near the thalamic synapse GABA-negative dendritic shafts frequently contained lamellar bodies, an organelle identical in structure to spine apparatus. Dendritic shafts and spines postsynaptic to the thalamocortical boutons frequently received an adjacent synapse from GABA-immunoreactive boutons.

The similarity between the magno- and parvicellular axons in their targeting of postsynaptic elements, including the GABAergic neurons, suggests that the structural basis of the physiological differences between 4Cα and 4Cβ neurons should be sought in other aspects of the circuitry of layer 4C, such as local cortical circuits, or in the far greater horizontal extent of the thalamocortical and GABAergic axons in layer 4Cα compared to those in the β subdivision.

Key words: visual cortex, thalamus, geniculocortical, intracellular recording, GABA, immunocytochemistry

Accepted May 26, 1989.

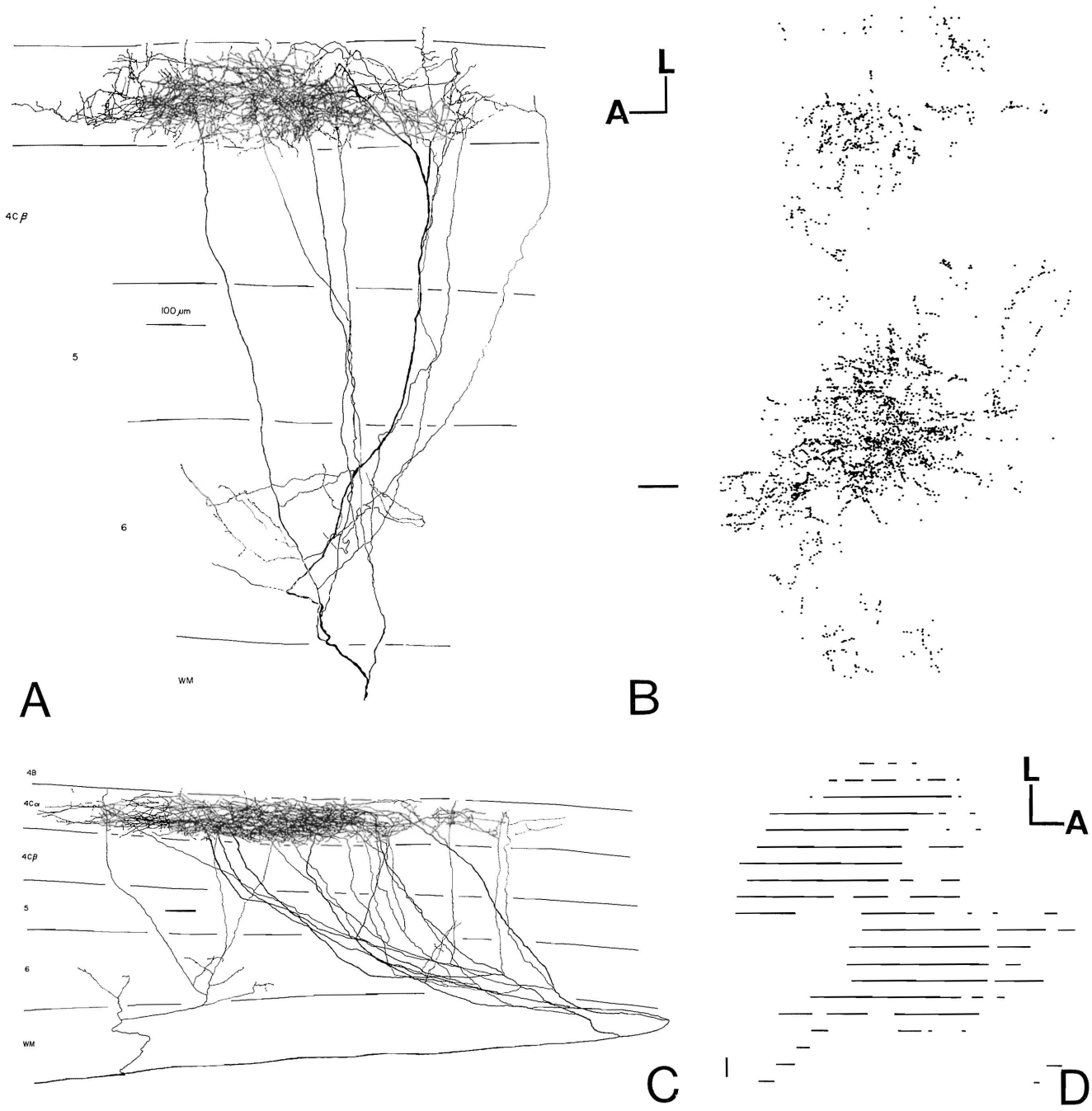

Fig. 1. **A,C:**Camera lucida reconstructions of two magnocellular axons (MA1 in A and MA2 in C) in the monkey striate cortex. They both had an off-centre receptive field. The centre size was 0.5° in diameter (MA1) and 1.6° × 1.1° (MA2) at a position of azimuth 7.5°, elevation −3.0° (MA1), and azimuth 0.9°, elevation −5.3° (MA2). Both axons were driven by the ipsilateral eye and responded well to low-contrast, broad-band stimuli. Surround antagonism was seen only for axon MA2. The terminal arbors are restricted to the upper part of layer 4C; only a few collaterals terminate in layer 6. **B:** Computer-assisted three-dimensional reconstruction of MA1. When viewed from the pia the boutons (dots) form three distinct clumps. **D:** Top view of axon MA2. Each line represents the extent of the arbor in a single 90 μm-thick Vibratome section. The drawings of each section were aligned and then, with 90 μm spacing, rotated 90° around the anterior-posterior axis. L, lateral; A, anterior; WM, white matter. Scales: 100 μm.

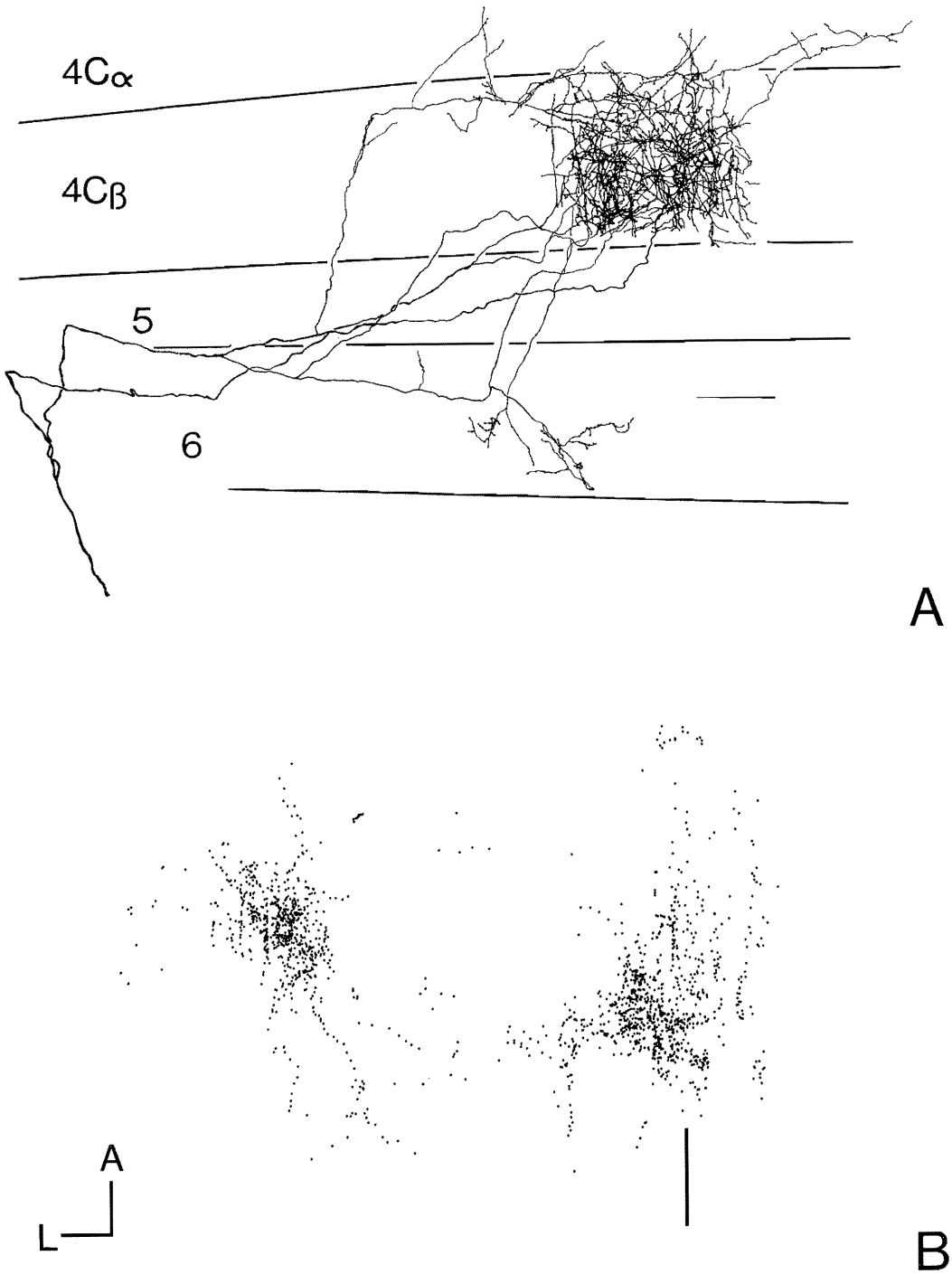

Fig. 2. **A:** Camera lucida reconstruction of a parvicellular axon (PA1) in the monkey striate cortex. It had an on-centre receptive field of 0.5° diameter in a position of asimuth 4.45° and elevation −3.85° and responded best to long-wavelength, high-contrast stimuli presented to the ipsilateral eye. No excitatory surround response could be elicited. The axon arborised mainly in layer 4Cβ, with only occasional collaterals entering layers 4Cα and 6. Note that the innervation of the lower half of layer 4Cβ is denser. **B:** Computer-assisted three-dimensional reconstruction of the axon seen in A; view of the boutons from the pia. Two distinct clumps are seen; they both are about 200 μm in diameter, with a centre-to-centre distance of around 400–450 μm. A, anterior; L, lateral. Scales: 100 μm.

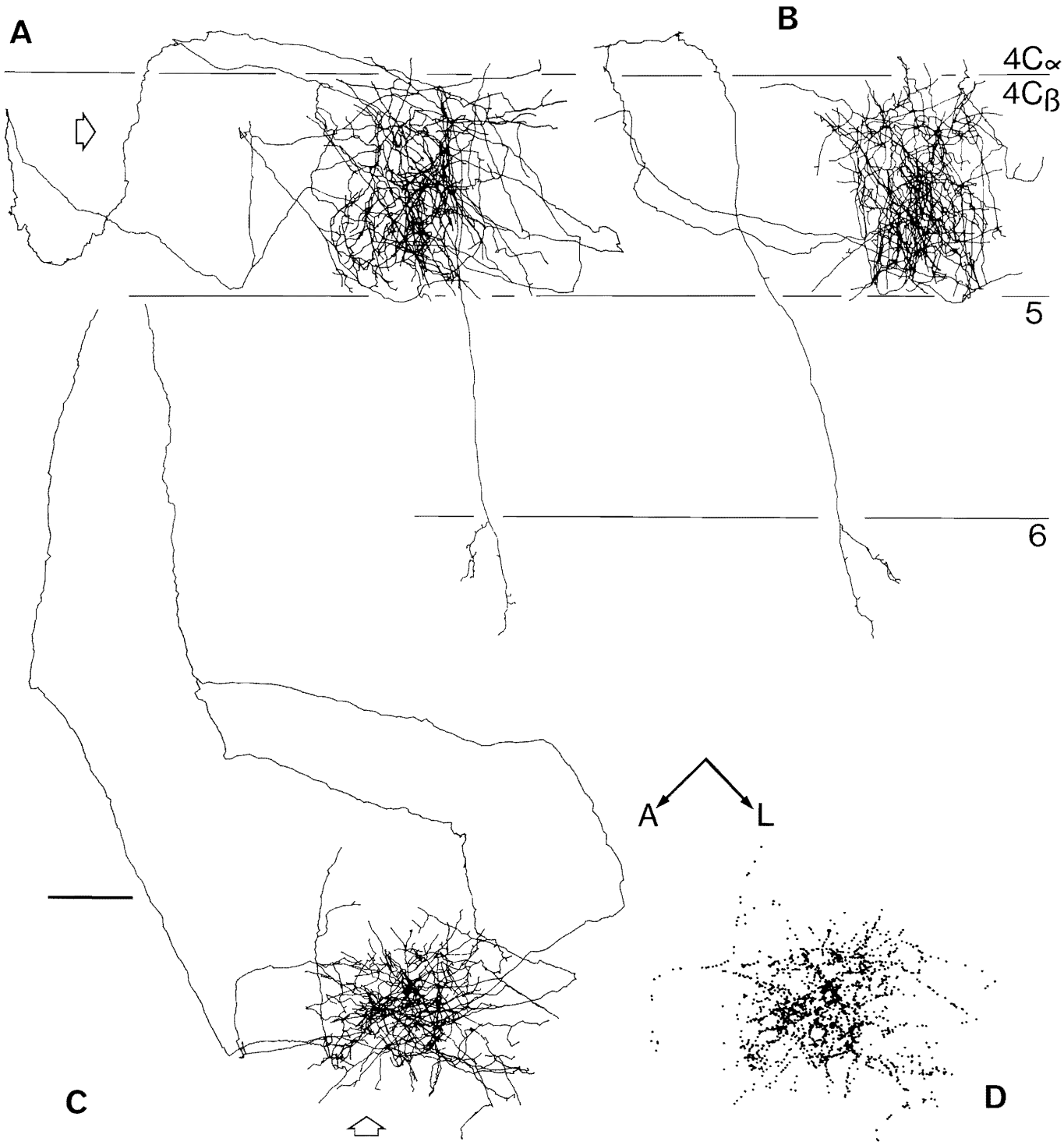

Fig. 3. Computer reconstruction of parvicellular axon PA2. It had an on-centre receptive field of 0.3° diameter in a position of asimuth 5.75° and elevation −3.3° and responded best to long-wavelength, high-contrast stimuli presented to the contralateral eye. No excitatory surround response or antagonism was detected. **A, B:** Two views as seen from directions parallel with the layers. Open arrow in A shows viewing direction to obtain the image in B after rotating the axon 90°. Note the sharp limits of lateral spread in the whole thickness of layer 4Cβ and the denser innervation of the lower half of the sublayer. Pia is to the top of figures in A and B. **C, D:** Views from the pia showing the arborisation pattern and the distribution of boutons, respectively. Arrows A and L show directions anterior and lateral respectively. Note that the majority of boutons are within a cylinder of around 150–200 μm in diameter. Open arrow in C shows the viewing direction to obtain the image in A, after rotating the axon 90°. Scale: 100 μm.

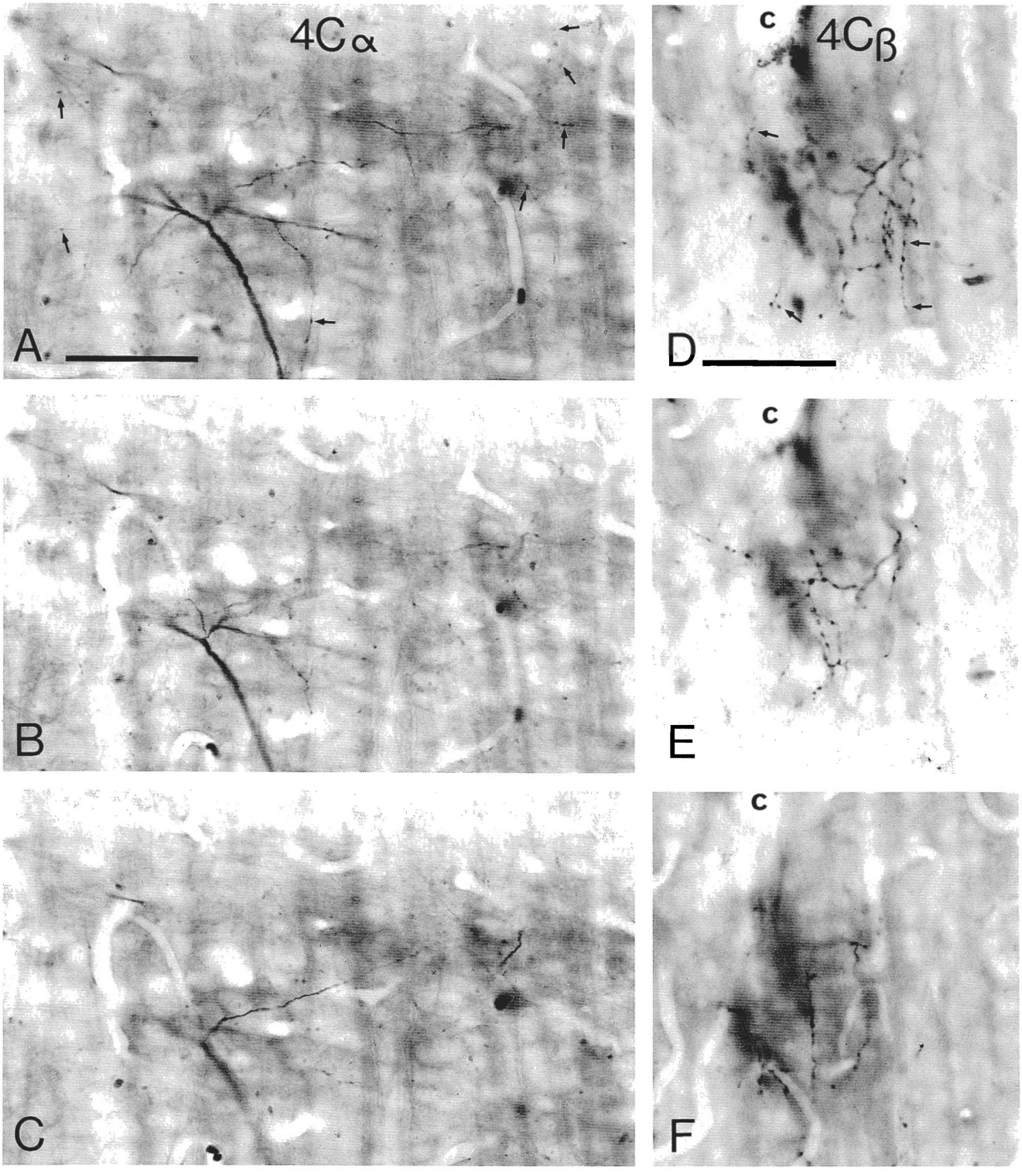

Fig. 4. **A–C:** Light micrographs of the magnocellular axon (MA2) shown in figure 1C. A small field of the arbor in layer 4Cα was photographed at three different focal depths. The HRP filling of this axon was relatively light; therefore in osmium-treated sections at low magnification some collaterals appear to be discontinuous. Arrows label some of the HRP-filled boutons of the axon. **D–F:** Light micrographs of the parvicellular axon (PA1) shown in Figure 2. A clump of the arbor in layer 4Cβ was photographed at three different focal depths. The boutons (arrows) are more densely packed than in the case of the magnocellular afferents. A capillary (c) is labelled as a landmark. Scales: 100 μm.

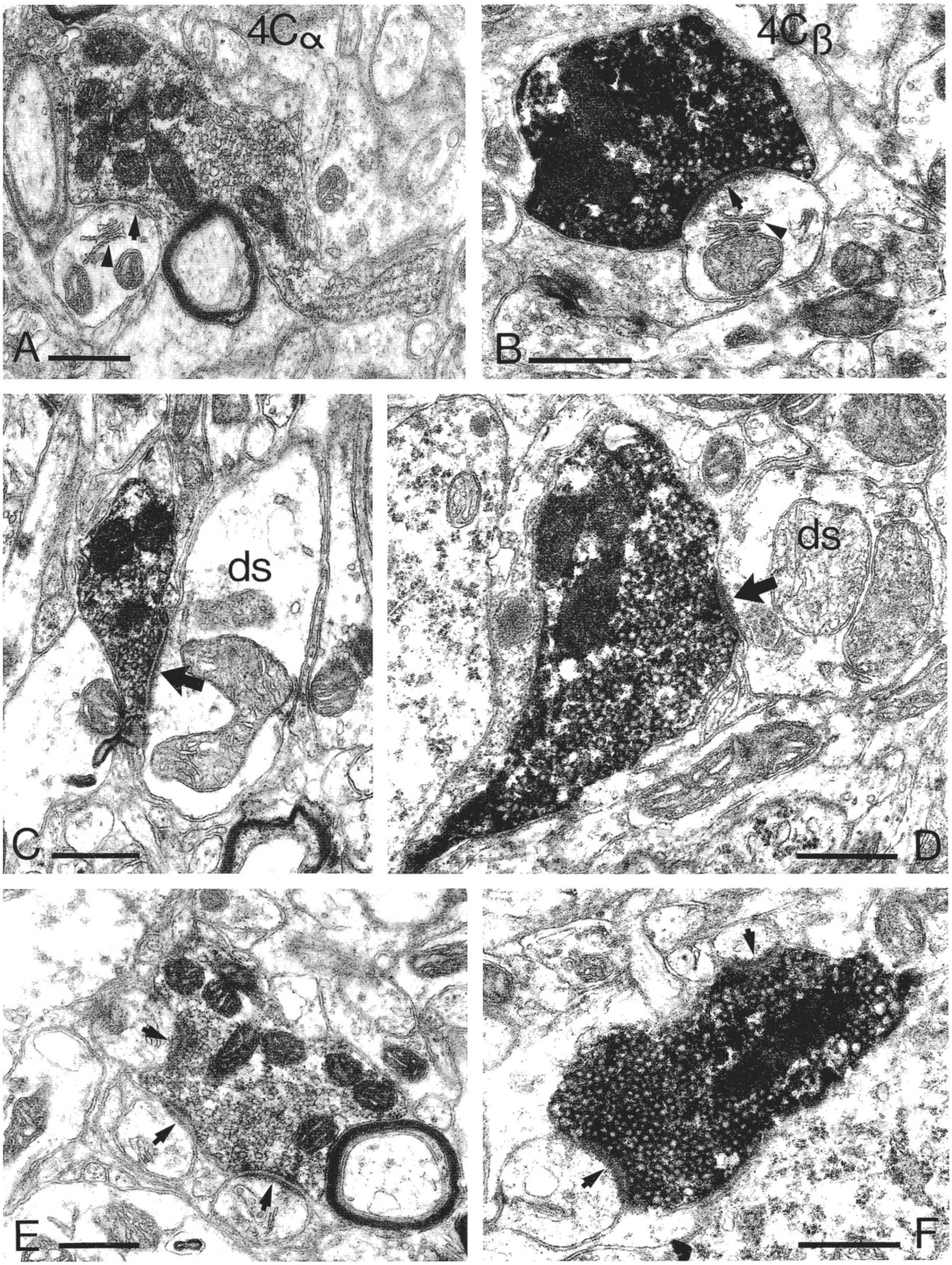

Figure 5

Ocular dominance columns, formed by the segregation of the left and right eye thalamic inputs to layer 4 of the visual cortex, thanks to studies of their organization, development, and modification by visual experience, have provided significant insights into the columnar organization of cortex (Hubel and Wiesel, '72; Hendrickson and Wilson, '78; for review see Hubel and Wiesel, '77). A great deal is known about the structural and functional organization of layer 4C, the main recipient zone of thalamic afferents. In Nissl-stained material layer 4C appears as a band densely packed with small neurons, which gives this cortical area its characteristic granular appearance. Golgi studies (Ramón y Cajal, 1899; Valverde, '71; Lund, '73, '87; Szentágothai, '73, '75; Lund and Boothe, '75; Mates and Lund, '83a) indicate that these neurons are spiny stellate cells and neurons with smooth dendrites. Pyramidal cells, the most common cell type in all other layers, are not found in layer 4C.

The upper portion of layer 4C (sublayer α) receives its input from the magnocellular layers of the lateral geniculate nucleus of the thalamus, whereas the lower portion (sublayer β) receives its input from the parvicellular layers (Hubel and Wiesel, '68; Hendrickson and Wilson, '78). The receptive field properties of neurons in these two divisions reflect their source of thalamic input (Hubel and Wiesel, '68, '72, '77; Dow, '74; Bullier and Henry, '80; Blasdel and Fitzpatrick, '84; Hawken and Parker, '84; Livingstone and Hubel, '84). The 4Cα cells are not sharply tuned to the stimulus wavelength and have high-contrast sensitivity, whereas many of the 4Cβ cells are wavelength-tuned and are less sensitive to contrast. All the layer 4C neurons tend to be strongly dominated by one eye. Originally it was thought that all neurons in layer 4C had nonoriented receptive fields resembling those of the lateral geniculate nucleus (Hubel and Wiesel, '68). Subsequently, a number of studies found orientation-selective cells in layer 4C with simple and complex receptive fields (Livingstone and Hubel, '84; Blasdel and Fitzpatrick, '84; Hawken and Parker, '84; Kennedy et al., '85). It now appears that most neurons in 4Cα are orientation sensitive. The nonoriented receptive fields in layer 4C are found for neurons in the β division. There is increasing evidence that these two subdivisions of layer 4C are part of at least two separate and parallel functional paths through the cortical areas (see rev. by Livingstone and Hubel, '87; Zeki and Shipp, '88; DeYoe and Van Essen, '88).

Much less detail is available about the synaptic organization of ocular dominance columns and layer 4C. The connections of different types of thalamic afferents are still poorly understood both in terms of their structure and in their contribution to the microcircuitry of layer 4C. Differences between layers 4Cα and 4Cβ have been found in the synaptic connections made by thalamic boutons in degeneration experiments (Winfield et al., '82; Winfield and Powell, '83). Magnocellular axons, on average, appeared to provide more synapses per bouton than parvicellular axons. Spiny stellate cells in layer 4Cβ have been shown to receive thalamic synapses (Kisvarday et al., '86), but only a few contacts have been identified, and cells in 4Cα have not been examined. Only one study has reported the distribution of physiologically identified arbors of the thalamic afferents in old-world monkeys (Blasdel and Lund, '83), but the synaptic connections made by single axons have not been studied.

The present study extends previous work on the arborisation patterns of single physiologically and morphologically identified afferents and in addition focuses on the synaptic connections made in the magno- and parvicellular recipient layers of 4C. Subtle differences have already been revealed in the cat in the synaptic organization of thalamic axons with different physiological properties (Freund et al., '85a,b). One would expect that the physiological differences between the α and β sublaminae might also be reflected in differences in the local circuitry within the laminae. In particular, GABA-mediated inhibition is thought to be important in controlling the response selectivity of cortical neurons to certain parameters of stimuli (for review see Sillito, '84). Therefore, we used immunocytochemical methods to determine the input from parvi- and magnocellular axons to GABAergic neurons in the cortex. The data provide new insights into the circuitry of layer 4C and will form a starting point for further studies on the development and plasticity of the microcircuitry of ocular dominance columns.

MATERIALS AND METHODS

Preparation of the animals, recording, and HRP injections

The material derives from two adult (weight: 5–6 kg) female monkeys (*Macaca nemestrina*). Anaesthesia was induced with ketamine hydrochloride (Ketalar, Parke-Davis). The saphenous vein and femoral artery were cannulated. Anaesthesia and analgesia were then maintained during sterile surgery with alfadolone acetate plus alfaxalone (SAFFAN; Glaxo) and a gas mixture of 1–2% halothane in a 70:30 mixture of N_2O and O_2. EEG, heart rate, blood pressure, temperature (38°C), and end-tidal CO_2 (5%) were continuously monitored. After paralyzing with 2 mg of pancuronium bromide (Pavulon, Organon Teknika) anaesthetic levels were assessed by using the EEG (slow-wave sleep) and blood pressure (approx. 100/70). Afocal contact lenses were placed over the corneas and correcting lenses were used to focus the eyes on the tangent screen, 1.14 m away. During electrophysiological recording the halothane was stopped and anaesthesia was maintained with sodium pentobarbital (minimum 2 mg/kg/hour). Pavulon was continuously infused at 0.5 mg/kg/hr.

A small craniotomy was made over area 17 and a plastic cylinder was cemented onto the skull. The dura was removed and the micropipette containing 4% horseradish peroxidase (HRP, Bohringer) and Tris-buffered 0.2 M KCl, with an impedance of 100 MΩ, was lowered onto the surface of the brain. The cylinder was filled with agar and sealed with wax to reduce pulsations. Neurons and axons were stimulated with hand-held stimuli. The wavelength of the stimulus was adjusted with gelatine or interference filters. Eye position was monitored with a reversible ophthalmoscope, which was used to project the position of the fovea onto the tangent screen.

Fig. 5. Postsynaptic targets of HRP-filled boutons of axon MA1 in layer 4Cα (A, C, E) and boutons of axon PA1 in layer 4Cβ. Note the asymmetrical synaptic specializations (arrows). The postsynaptic dendritic shafts belonged to two major types. Dendrites of one type (in **A, B**) were of medium to small caliber, had small dark mitochondria, and often contained lamellar bodies (arrowheads in A, B). Occasionally, they bore spines. The other type of shafts (ds, **C, D**) contained large mitochondria, did not possess lamellar bodies or spines, and were occasionally varicose. **E, F:** The predominant targets of both the magnocellular (E) and the parvicellular (F) boutons were dendritic spines. A single bouton often contacted several spines. Scales: A–F, 0.5 μm.

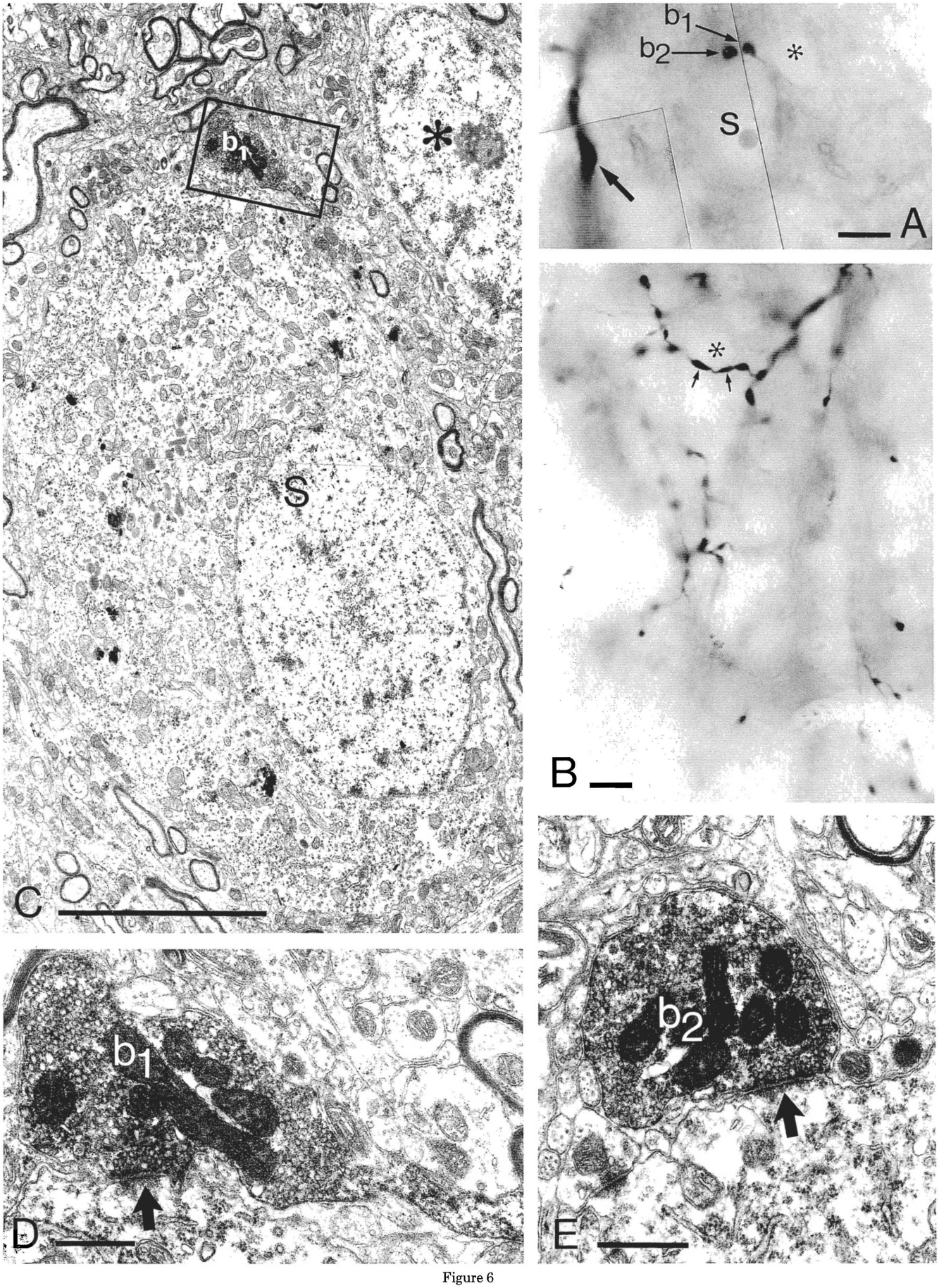

Figure 6

In classifying the neurons and fibres we concentrated on those properties that could be assessed by using hand-held stimuli. For the afferent fibres we drove the pipette into the white matter underlying the cortex. Axons were first recorded extracellularly and their receptive fields were plotted. Parvicellular axons were identified by their monocular nonoriented receptive fields, their sensitivity to the wavelength of the stimulus, and by their poor response to stimuli of low contrast (Shapley et al., '81) and to large, fast-moving stimuli of opposite contrast to the centre. Magnocellular axons were identified by their monocular nonoriented receptive fields, their good response to a wide range of wavelengths, and by their ability to respond briskly to low-contrast stimuli and to large, fast-moving stimuli of opposite contrast to the centre. Both magno- and parvicellular axons had high spontaneous activity that could usually be inhibited by stimulating the centre with a stimulus of inappropriate contrast or wavelength. The spatial extent of the receptive field centre was plotted by using flashed light spots to which both magno- and parvicellular axons responded briskly. After mapping the receptive field the axon was repeatedly stimulated with an optimal stimulus while the pipette was advanced in an attempt to impale the fibre. On the occasions when the fibre was impaled, as indicated by a sharp drop in the DC potential of about 40 mV, the receptive field was remapped and the fibre was then injected with HRP by using depolarizing current pulses (2–4 nA) for several minutes, or as long as it was possible to retain intraaxonal recording.

Perfusion, peroxidase histochemistry, and embedding

Two to 12 hours after the injection of HRP the monkey was given an overdose of barbiturate and perfused through the heart with saline followed by 2.5% glutaraldehyde and 1% paraformaldehyde. Blocks of area 17, thought to contain the HRP-filled afferents, were dissected and sectioned on a Vibratome (Oxford Instruments) at 80 μm. The histochemistry for HRP was performed according to Hanker et al. ('77) by using the pyrocatechol/p-phenylene diamine reaction with cobalt and nickel intensification (Adams, '81). Well-filled axons were selected from wet sections under the light microscope and treated with 1% osmium tetroxide for 40 minutes. The sections were then dehydrated in ethanol (1% uranyl acetate was included in the 70% ethanol step for 40 minutes), embedded in resin (Durcupan ACM, Fluka), mounted on microscope slides under a coverslip, and cured at 56°C for 2 days.

Fig. 6. **A, B:** Light micrographs of somatic contacts established by magnocellular (A) and parvicellular (B) axon terminals. A: Two boutons (b_1, b_2) of the magnocellular axon are in contact with a large cell body (S). The arrow points to a main axon trunk. A small cell body (asterisk, see also in C) serves as a landmark for correlation with the electron micrograph shown in C. **C:** One of the boutons (b_1) establishes an asymmetrical synaptic contact (arrow in D) with the cell body. The framed area is shown in **D. E:** The other bouton (b_2), also shown in A, is in asymmetrical synaptic contact (arrow) with the cell body. B: Two boutons (arrows) of the parvicellular axon are in contact with a small cell body (asterisk). Electron microscopy showed that there were no synaptic contacts between the HRP-filled terminals and this cell body. Scales: A, B, 10 μm; C, 5 μm; D, E, 0.5 μm.

Two- and three-dimensional reconstruction of HRP-filled axons

The HRP-injected axons were drawn first by using a drawing tube and then digitized by using two different three-dimensional neuron reconstruction systems. Axon PA2 (Fig. 3) was digitized by feeding the X, Y, and Z coordinates with 0.5 μm accuracy (100 × oil immersion objective) into an IBM AT computer by using a neuron reconstruction system (Neutrace) and software programs NEURON, NEUMER, NEUROT, and NRN11A and statistical programs (Zsuppan, '84). Two other axons (PA1 and MA1) were reconstructed by using the Neuroscience Research Centre Cell Reconstruction Facility, University of Alabama in Birmingham. The system employs a VAX 11/750 computer, Evans & Sutherland PS 300 display unit, and software developed in house. Processes were digitized in three dimensions with 0.1 μm accuracy at 1,000× magnification (100× oil objective) by using a drawing tube attachment and a bitpad. Section alignment of the 80 μm-thick sections was achieved by using a docking program that allowed simultaneous display of serial sections from any viewpoint. An interactive program was then used to align the section by using fiducial marks such as the cut ends of the HRP-filled processes.

Electron microscopy and postembedding immunogold staining for GABA

Selected portions of the HRP-filled axon arborisations were photographed in the light microscope, re-embedded (Somogyi et al., '79), and serially sectioned for electron microscopy. The serial ultrathin sections were mounted alternately on Formvar-coated copper and gold grids (four to six sections on a copper and two or three sections on a gold grid). The copper grids were stained with lead citrate (Reynolds, '63) and the gold grids were processed for postembedding immunogold staining by using an antiserum against GABA.

The procedure followed that of Somogyi and Hodgson ('85) with modifications (Somogyi and Soltesz, '86). Briefly, the following steps were carried out at room temperature on droplets of solutions (all Millipore filtered, pore size 0.22 μm) placed on Parafilm in petri dishes unless otherwise stated: 1% periodic acid for 7–10 minutes; three washes in distilled water by dipping followed by 5 minutes on drops; 1% sodium metaperiodate for 7–10 minutes; 2 × 10 minutes in Tris (10 mM)-phosphate (10 mM)-buffered isotonic saline (TPBS), pH 7.4; blocking of nonspecific reaction with 1% ovalbumin in TPBS for 30 minutes; quick rinse in dd·H_2O; 1% normal goat serum (NGS, in TPBS) for 5 minutes; antiserum to GABA for 1–2 hours (code No. 9, Hodgson et al., '85), diluted with 1% NGS in TPBS at 1:1,000 to 1:3,000; 3 × 15-minutes wash in 1% NGS; 5 minutes in 1% polyethylene glycol (mol. wt. 15,000–20,000, Sigma) dissolved in 50 mM Tris buffer (pH 7.0); Goat antirabbit IgG-coated colloidal gold (15 nm, Janssen Life Sci. Prod.) diluted at 1:10 to 1:40, for 2 hours; three dips plus 10 minutes in dd·H_2O; staining with 1% uranyl acetate in distilled water for 30 minutes; three dips in dd·H_2O; staining with lead citrate; three dips in dd·H_2O.

Some of the osmium is removed from the sections during the immunostaining procedure, and the HRP-filled profiles lose their electron density. Therefore, HRP-filled boutons had to be identified on alternate grids, which were not processed for immunogold staining. The same boutons were

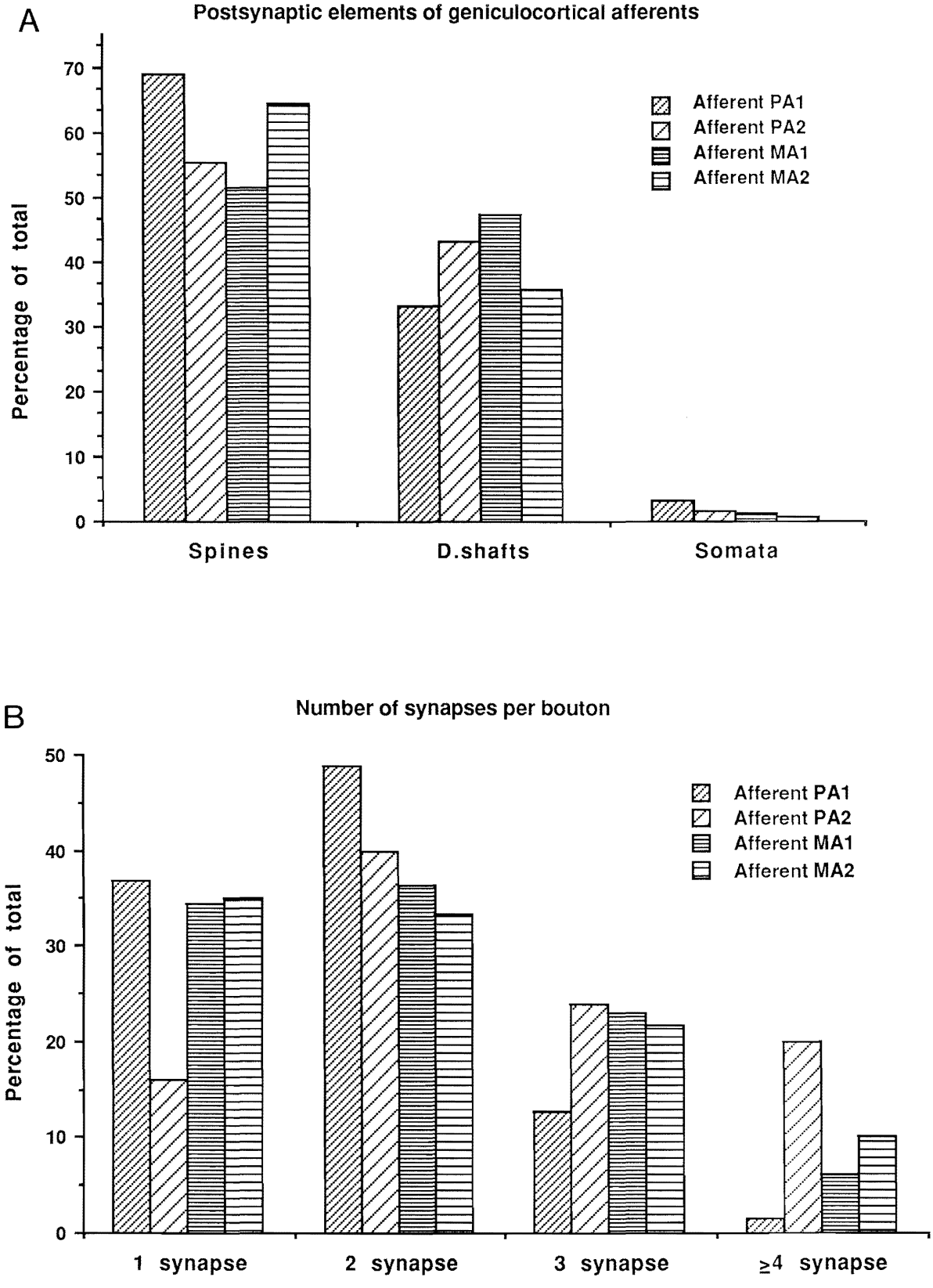

Fig. 7. Quantitative distribution of the types (**A**) and number (**B**) of postsynaptic elements for the magnocellular (MA1 and MA2) and the parvicellular (PA1 and PA2) axons was established by reconstruction of boutons (113 of MA1, 60 of MA2, 125 of PA1, and 25 of PA2) in the electron microscope from serial ultrathin sections.

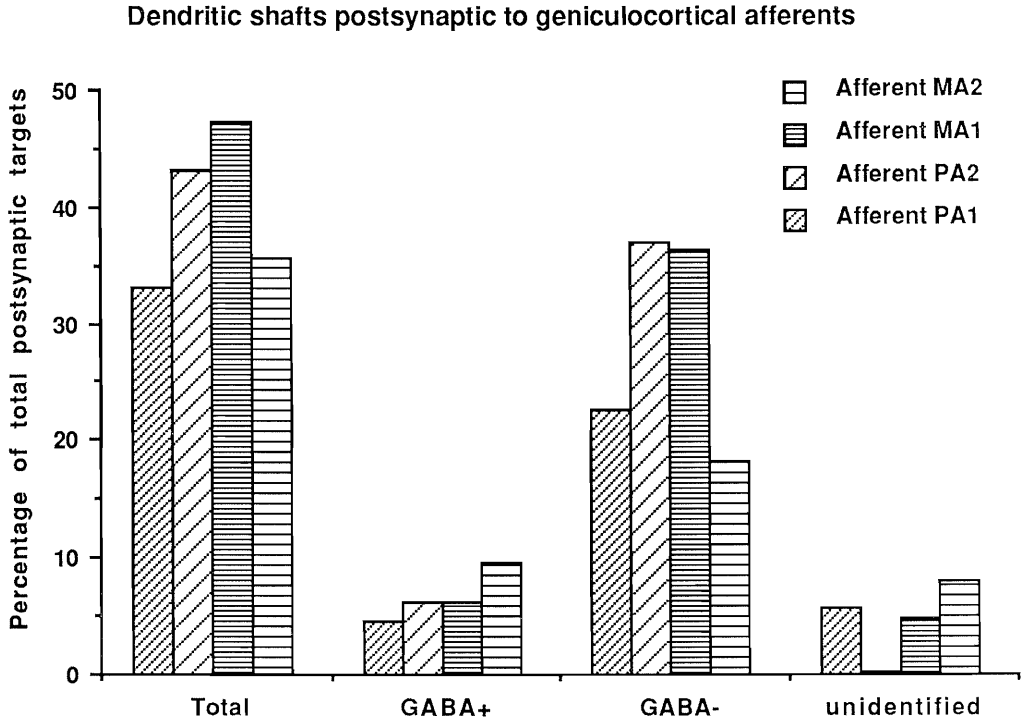

Fig. 8. Distribution of GABA-negative, GABA-positive, and uncategorized dendritic shafts postsynaptic to axons MA1 (108 dendritic shafts, 47.2% of total targets), MA2 (45 dendritic shafts, 35.7% of total targets), PA1 (74 dendritic shafts, 33.0% of total targets), and PA2 (28 dendritic shafts, 43.1% of total targets).

then searched in sections on neighbouring immunostained grids by using capillaries, somata, or other large profiles as landmarks.

RESULTS

Electrophysiological features of geniculocortical axons

The axons were electrophysiologically identified on the basis of criteria outlined in the Materials and Methods section. Both parvicellular axons had on-centre receptive fields that responded best to long-wavelength stimuli. The magnocellular axons had off-centre receptive fields and could be activated by broad-band stimuli. One of the parvicellular axons (PA1) and both magnocellular axons were driven by the ipsilateral eye, and the other parvicellular axon (PA2) was driven by the contralateral eye. Further details of the receptive fields are given in the figure legends for the individual axons.

Light microscopic features and three-dimensional reconstruction

Two magnocellular (MA) and two parvicellular (PA) axons, well filled with HRP, were used for the light and electron microscopic analysis.

The MA axons arborised in a dense narrow band within layer 4Cα; the innervation of layer 6 was very sparse (Fig. 1). The main axon trunks branched to several major collaterals before leaving the white matter. Even these collaterals were large in diameter, approximately 3–4 μm at the point of entry to the cortex (not corrected for tissue shrinkage). Only a few of the collaterals gave short sidebranches in layer 6. Occasional collaterals appeared to enter layers 4Cβ and 4B, but even these remained restricted to the laminar boundary regions (Fig. 1). The exact boundary between 4Cα and 4Cβ was estimated to be at half the width of layer 4C. In layer 4Cα the axons gave rise to finer branches, which were studded with large en passant boutons (average diameter 1–2 μm). Clusters of boutons, or obvious associations with any particular target profiles, were rare. A few somata (three to five per axon) were nevertheless seen to receive multiple contacts. The terminal fields in layer 4Cα of both MA axons appeared homogeneous on the camera lucida drawings (Fig. 1A,C); however, the three-dimensional reconstructions revealed that each arborisation consisted of three clumps best seen when viewed from the pia (Fig. 1B,D). The two large clumps were clearly separate, but the third clumps of both axons were very small and could be regarded as extensions of the large clumps. The two larger clumps were 300–500 $\times$ 600–1,200 μm in size, elongated obliquely in the anterior-posterior direction, and had a centre to centre spacing of 800 μm. The dimensions and spacing of these clumps suggest that they correspond to ocular dominance columns. Axon MA1 had 3,200 boutons; those of MA2 were not counted, but there appeared to be approximately twice as many.

The PA axons formed a very dense arborisation in layer 4Cβ, and a few collaterals were seen in layer 6 as well,

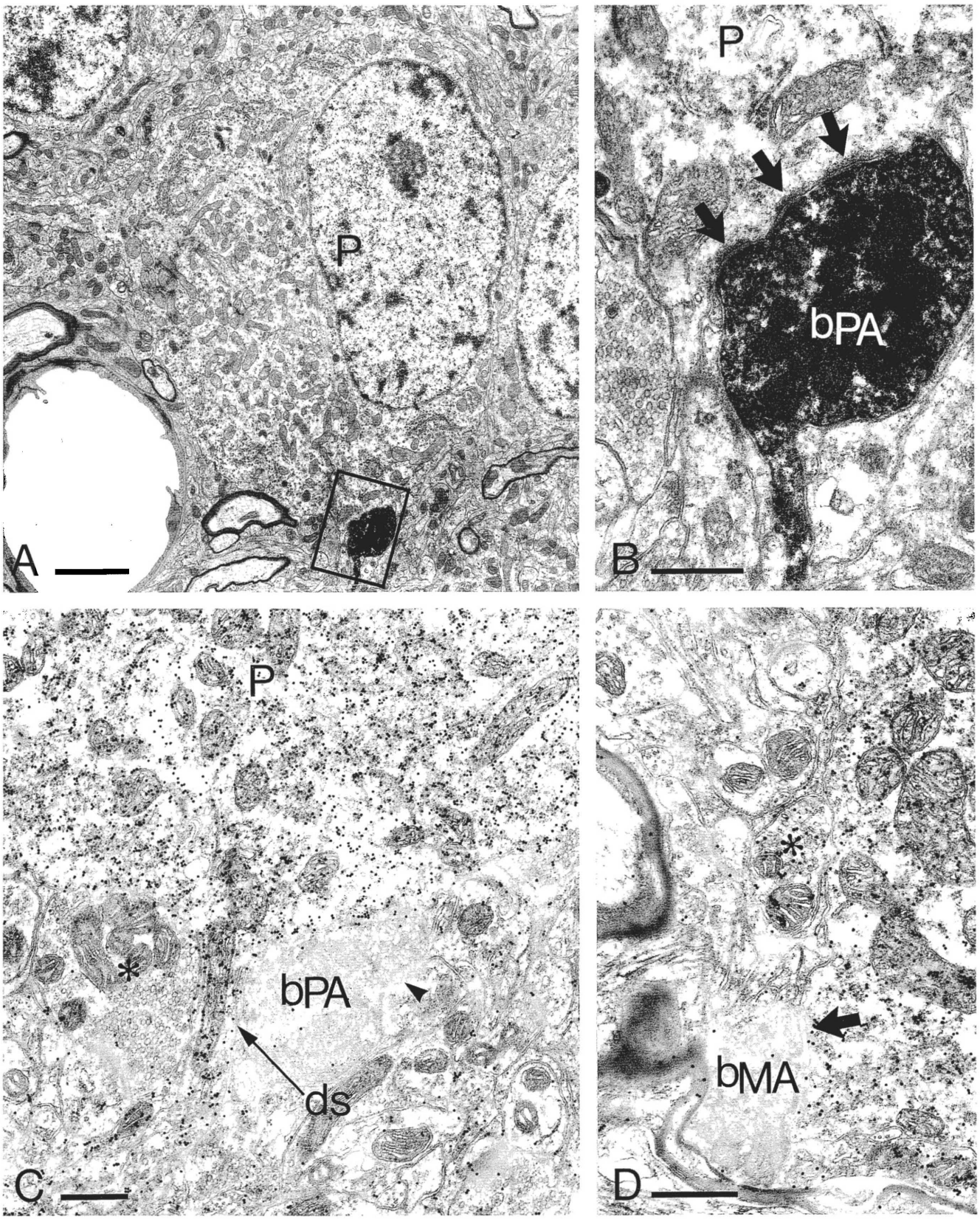

Fig. 9. **A, B:** A bouton (framed area in A, shown at higher power in B, b_{PA}) of axon PA1 is in asymmetrical synaptic contact (arrows in B) with a cell body (P). **C:** The GABA immunoreactivity of the perikaryon was tested on alternate grids by the immunogold technique and is shown here a few sections away in the series. The high concentration of gold particles over the cell body and its dendrite (ds) shows that it is positive for GABA. The HRP-filled bouton is much less electron-dense in this section because of the partial removal of osmium during the immunostaining procedure. The parvicellular bouton (b_{PA}) in this section contacts a spine (arrowhead). **D:** An HRP-filled terminal (b_{MA}) of a magnocellular axon (MA1) in asymmetrical synaptic contact (arrow) with a cell body, which is immunoreactive for GABA as shown by the accumulation of gold particles. Another bouton not labelled with HRP (asterisk) is also GABA-positive. Scales: A, 2 μm; B–D, 0.5 μm.

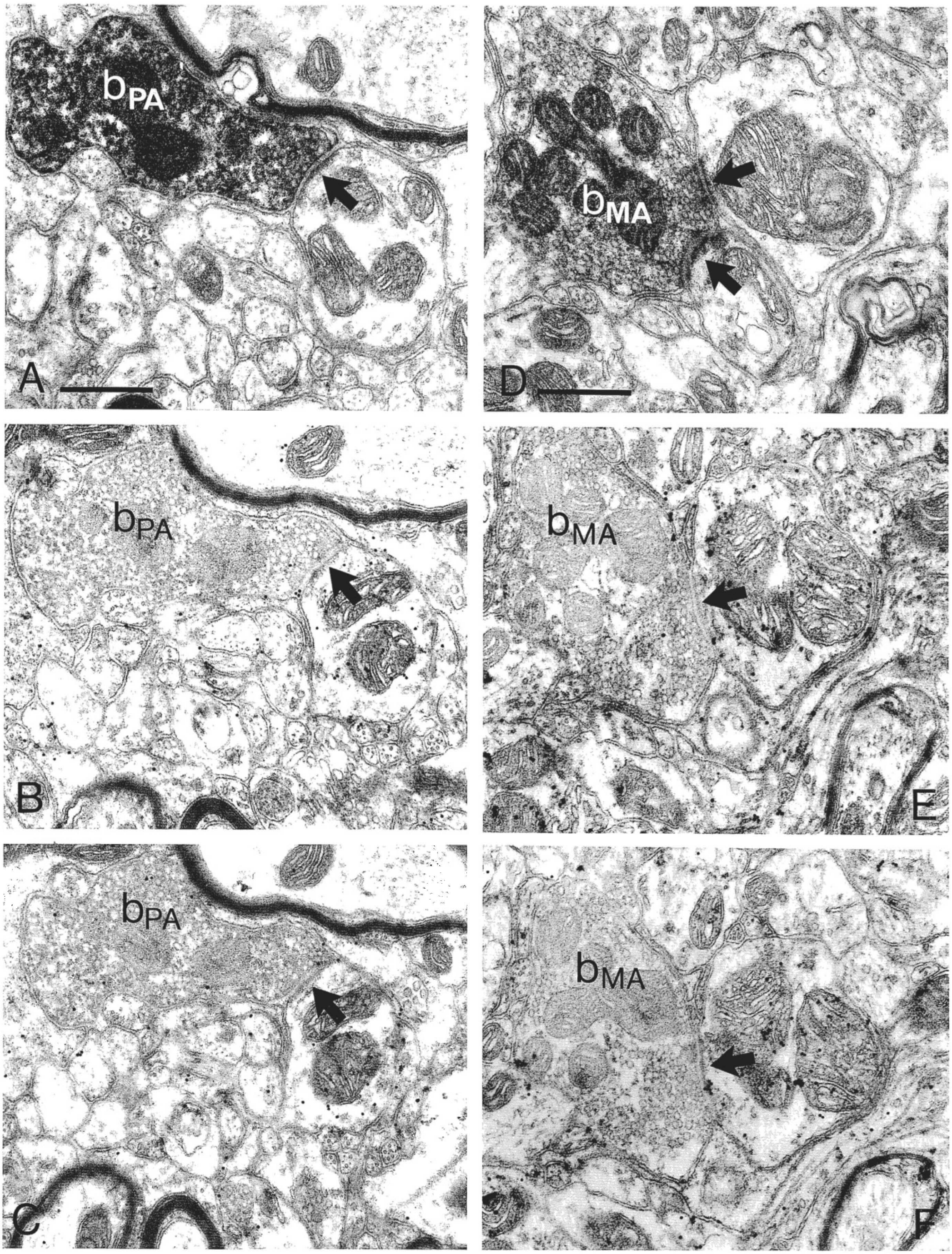

Fig. 10. **A–C:** A parvicellular axon terminal (b_{PA}) in asymmetrical synaptic contact (arrow) with a dendritic shaft. Serial sections of the same area were immunostained for GABA (B, C). The accumulation of gold particles shows that the dendritic shaft is immunoreactive for GABA. **D–F:** A magnocellular axon terminal (b_{MA}) forming an asymmetrical synaptic contact (arrows) with two dendritic shafts. The upper dendritic shaft is immunoreactive for GABA, as shown by the accumulation of gold particles in serial sections in E and F. Scales: A, D, 0.5 μm.

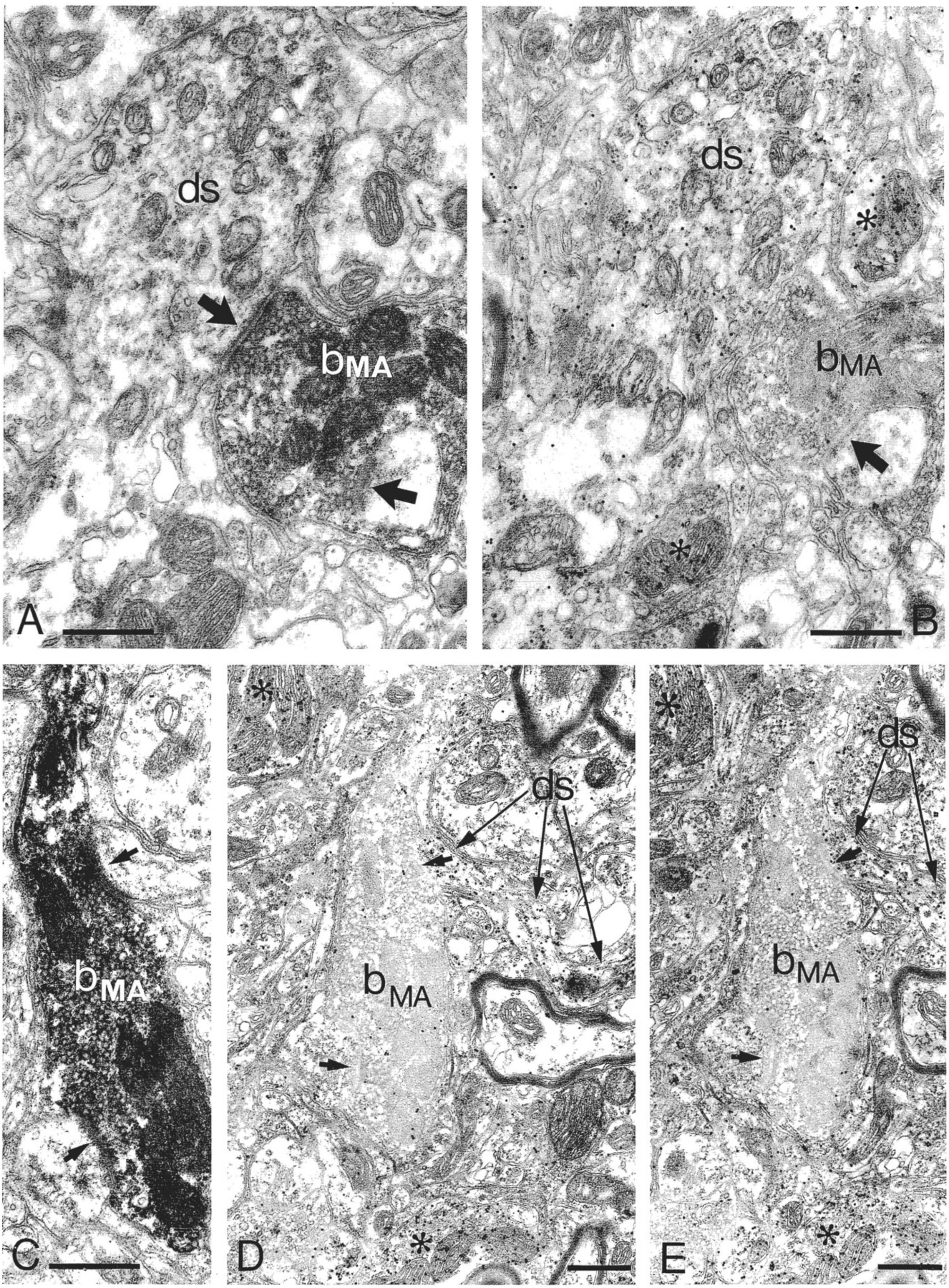

Figure 11

radially below the layer 4 arbor (Figs. 2, 3). The layer 4Cβ clump had sharp borders with layers 5 and 4Cα, and collaterals entering the lower half of layer 4Cα were sparse. On the camera lucida drawings both PA axons appear to have a tangentially homogeneous distribution of collaterals in layer 4Cβ (Figs. 2A, 3A,B). However, the top views obtained by computer-assisted three-dimensional reconstructions revealed that one of the PA afferents (PA1) arborised in two distinct clumps (Fig. 2B); each clump was about 150–200 μm in diameter and had a centre-to-centre spacing of 450 μm. The other axon (PA2) had a single clump of 150–200 μm diameter with sharp limits of lateral spread, giving it the box-like appearance seen on the computer rotation (Fig. 3B). The density of collaterals and varicosities was higher in the lower than in the upper half of 4Cβ. The parvicellular arbor had fewer boutons (PA1: 1,520; PA2: 1,380) than the magnocellular arbors. Interestingly, the number of boutons formed by the two PA axon is very similar in spite of the difference in the number of clumps they formed.

The main axons were thinner (1–3 μm) than those of the MA axons. The PA axons appeared to have far more boutons per unit volume than the MA afferents (Figs. 2, 3, 4D–F). In layer 4Cβ the main axons gave rise to several fine collaterals that were studded with en passant boutons with interbouton intervals smaller than those of the MA axons. Associations of the boutons with particular target profiles were not seen. Contacts on cell bodies were frequent, but this was the result of the high packing density of somata in this layer. The majority of these somatic appositions were found to lack synaptic specializations, as shown by electron microscopy (see below).

Ultrastructural characteristics of geniculocortical axons and their postsynaptic targets

Thick sections containing large numbers of HRP-filled boutons from different parts of the MA and PA arborisations were re-embedded and sectioned for electron microscopy (EM). All smooth branches of the axons were heavily myelinated. The finer collaterals only lost their myelin sheath just before the formation of the first synaptic bouton. The large boutons along these fine collaterals seen in the light microscope were invariably found to form synapses when examined in the EM. They contained several rather small-diameter mitochondria and were filled with round synaptic vesicles (Figs. 5A,E, 6D,E). All synaptic contacts established by these identified thalamic axons were clearly asymmetrical (Gray's type 1) when studied in serial sections. Occasionally, in single sections, the postsynaptic membrane specialisation appeared very thin near the edge of the synaptic specialization and could have been misinterpreted as a symmetrical (Gray's type 2) synapse. A total number of 150 PA and 173 MA boutons were studied in serial sections and reconstructed in the electron microscope. The number of synapses per bouton and the types of postsynaptic targets have been established for each bouton (Fig. 7) from serial section reconstruction. The postsynaptic targets were also tested for the presence or absence of GABA by using immunocytochemistry (Fig. 8). All postsynaptic profiles lacking mitochondria and microtubules were classified as dendritic spines, and all those that contained mitochondria and/or microtubules were classified as dendritic shafts, irrespective of their diameter. A large proportion of the target dendritic shafts had small diameters and looked like spines, especially those containing lamellar bodies (see below). In order to confirm that the presence or absence of mitochondria can be used as a criterion to distinguish spines and shafts, we reconstructed in serial EM sections 36 spine heads of five Golgi-impregnated spiny stellate cells from area 17 of a monkey. None of these spines contained mitochondria.

The MA and PA axons terminated on a similar range of postsynaptic targets, which included dendritic spines and shafts and cell bodies (Fig. 7A). Axon PA1 contacted a slightly higher proportion of dendritic spines (68.9%) and fewer dendritic shafts (33%) than the other PA axon (PA2, 55.4% spine and 43.1% shaft). The MA axons also differed from each other, MA2 contacting a higher proportion of spines (64.3%) and lower proportion of dendritic shafts (35.7%) than axon MA1 (51.5% spines and 47.2% shaft). Thus, there is a greater similarity in the distribution of postsynaptic targets between MA2 and PA1 or between MA1 and PA2 than between axons of the same physiological type.

When a bouton contacted dendritic spines, it usually contacted several of them (Fig. 5E,F). Most of the spines contained a spine apparatus. The target dendritic shafts were of two distinct types. One type was of larger diameter and, in general, contained larger mitochondria (Figs. 5C,D, 10, 11), whereas the other type had smaller diameter, smaller mitochondria, and frequently contained a lamellar body, which is an organelle similar in structure to the spine apparatus (Figs. 5A,B, 12).

Perikarya accounted for a very small proportion of the targets of both types of afferent (3.1% of the PA1, 1.5% of the PA2, 1.3% of the MA1, and none of the examined MA2 targets). Most postsynaptic perikarya showed the ultrastructural features of nonpyramidal cells: e.g., high nucleus/cytoplasm ratio; abundance of large mitochondria, rough endoplasmic reticulum, and free ribosomes; and both symmetrical and asymmetrical synaptic input (Figs. 6C, 9A). The eight somatic synapses given by one of the PA axons (PA1, Fig. 2) were distributed on five perikarya, four of which were in the clump studied in greater detail. The position of these somata was rather peculiar; two of them were at the anterior and the other two at the posterior edge of the clump. The other PA axon (PA2, Fig. 3) contacted a single cell body, the fine structural features of which were indistinguishable from those of spiny stellate cells. Only a single cell body was contacted by three boutons of the 125 sampled from one of the MA axons (MA1, Fig. 1A), and none of the 60 boutons sampled from MA2 (Fig. 1C) terminated on somata.

There was a large scatter among the axons also with respect to the number of synapses per bouton. Axon PA1 established less synapses per bouton (1.79) than the MA axons (2.03 for MA1 and 2.1 for MA2). The other parvicellular axon (PA2), however, established far more synapses per

Fig. 11. **A, B:** A magnocellular bouton (b_{MA}) of axon MA1 in asymmetrical synaptic contact (arrows) with a large proximal dendrite (ds) and a spine (lower thick arrow). The dendritic shaft as well as two axon terminals (asterisks) is positive for GABA on a consecutive immunostained section (B). **C–E:** A small-caliber dendrite (ds, upper right) and a spine (lower left) receive asymmetrical synapses (arrows) from an HRP-filled bouton (b_{MA}) of a magnocellular afferent (MA1). The thin dendritic shaft (ds) and two boutons (asterisks) are strongly immunoreactive for GABA, whereas the spine is immunonegative. Scales: A–E, 0.5 μm.

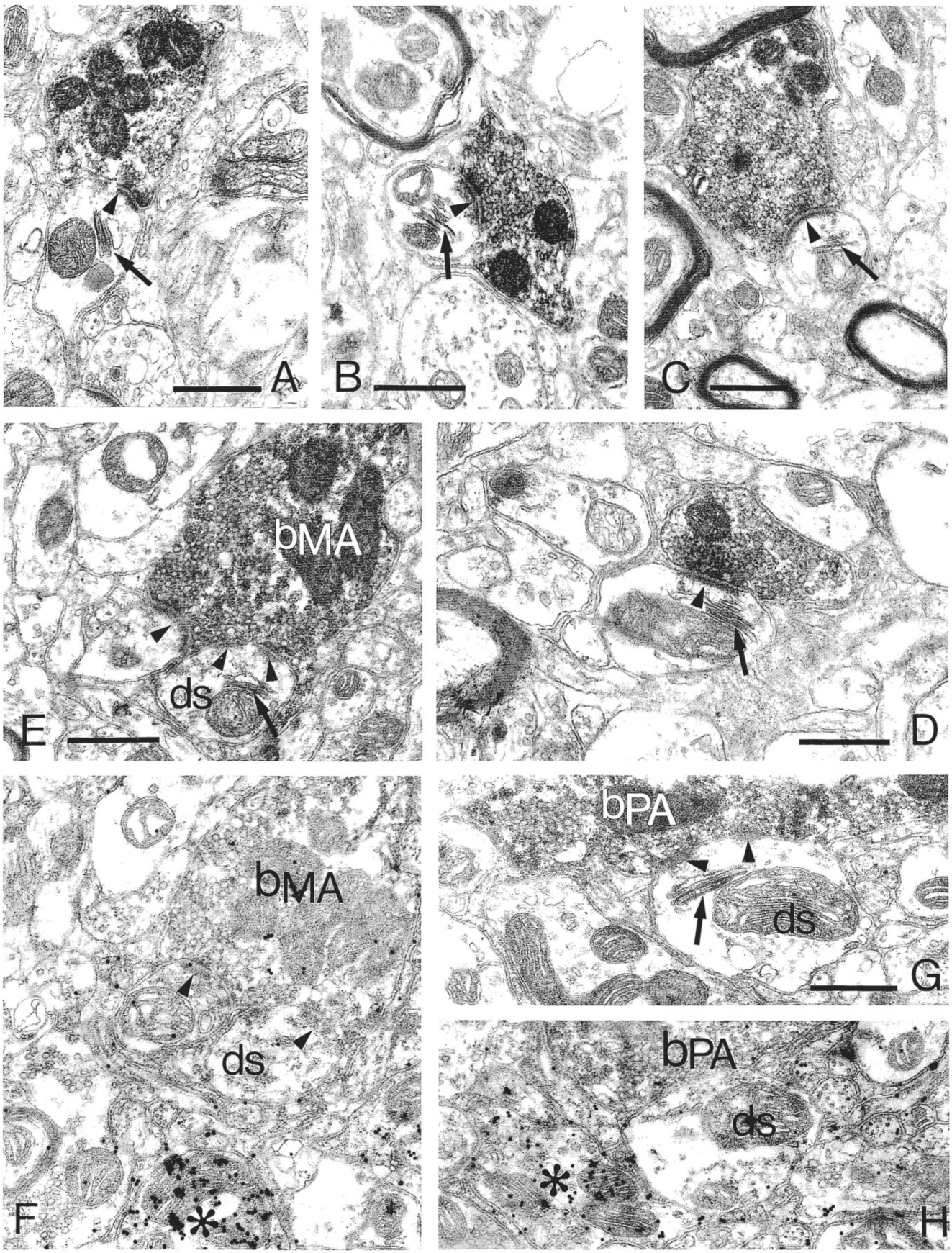

Figure 12

bouton (2.6) than any of the other three axons. The proportion of boutons establishing one, two, three, and four or more synapses is shown in a histogram in Figure 7B. The majority of boutons of both types of afferents established one or two synapses, but giant boutons (up to 3 μm in diameter) contacting four to six postsynaptic targets (mostly small spines) were also seen.

Identification of postsynaptic targets by GABA immunocytochemistry

The pattern of GABA immunoreactivity was similar to that described earlier in the visual cortex of cats and monkeys (Hendrickson et al., '81; Freund et al., '83; Fitzpatrick et al., '87; Hendry et al., '87). The majority of the boutons containing flat vesicles and making symmetrical synapses were positive for GABA, as were dendritic shafts and somata showing the characteristics of nonpyramidal neurons (see above). The difference in gold particle density between positive and negative profiles was so striking that quantification was unnecessary. The level of background staining varied from incubation to incubation, but even at relatively high background levels the accumulation of gold particles above the immunoreactive structures was distinct (Fig. 9C). Grids with poor immunostaining were excluded from the sample. The HRP-filled terminals lose their electron density during the sodium periodate treatment of the immunostaining procedure. Therefore, the boutons were mapped first in a nonimmunostained section, and then, using capillaries, somata, or other large-diameter profiles as landmarks, they were identified in the neighbouring immunostained sections. HRP-filled boutons of both the MA and PA afferents were always negative for GABA (Figs. 9–13).

All postsynaptic spines were negative (Figs. 11, 13C–F) and all postsynaptic somata were positive for GABA (Fig. 9C,D). The GABA immunoreactivity of dendrites is usually weaker than that of synaptic boutons or perikarya. Therefore, the immunoreactivity of target dendrites was always assessed from several (two to six) consecutive ultrathin sections of the same profile. The proportion of all postsynaptic dendritic shafts and, of these, the proportion of GABA-positive, GABA-negative, and unidentified (i.e., because of unsuccessful immunostaining of the alternate sections) dendrites is shown in a histogram (Fig. 8). GABA-positive dendritic shafts represented 6.2% (14 out of 229) of the total number of targets of MA1, 9.5% (12 out of 126) of MA2, 4.5% (ten out of 224) of one clump of PA1, 3.8% (two out of 53) of the other clump of PA1, and 6.2% (four out of 65) of PA2. Thus, MA1 contacted exactly the same proportion of GABAergic dendrites as PA2 and differs from PA1 not more than from MA2. From all the postsynaptic targets the proportion of GABA-negative dendrites was 36.2% for MA1, 35.7% for MA2, 22.8% for PA1, and 36.9% for PA2. The remaining small proportion of the postsynaptic dendritic shafts were not categorized as GABA-positive or -negative (Fig. 8).

The proportion of GABA-positive dendritic shafts should be considered as a minimum number, since the possibility of false negativity cannot be excluded in immunostaining. Nevertheless, the GABA-negative shafts had other features in common; e.g., they often contained lamellar bodies (see below) or gave rise to spines. This suggests that the lack of GABA immunoreactivity in these dendrites was genuine. The GABA-positive dendritic shafts also had ultrastructural features in common. In general, the mitochondria in GABA-positive profiles were larger and appeared to have a light matrix compared to the mitochondria in non-GABAergic profiles (Figs. 6, 9, 10D–F, 11A,B). The GABA-positive dendritic shafts were often thick proximal dendrites (Fig. 11A,B) but thin distal dendrites were also found (Fig. 11C–E).

Dendritic shafts containing lamellar bodies were never found to be immunoreactive for GABA (Fig. 12E–H). The lamellar bodies were similar in structure to the spine apparatus; they were usually positioned between a mitochondrion and the postsynaptic specialization of the thalamic synapse; and they were apposed to the membrane of the mitochondrion (Figs. 5A,B, 12). Often the membrane-limited saccule facing the thalamic synapse was more swollen than the inner saccules, and electron-dense material could be seen between the outer saccule and the postsynaptic membrane specialisation (Figs. 5B, 12E,G).

The synapses established by either PA or MA boutons onto small-caliber dendrites or spines were frequently associated with a symmetrical synapse terminating on the same structure, and these symmetrical synapses were always positive for GABA (Fig. 13). Such a synaptic arrangement was seen in case of 10–20% of the thalamocortical synapses. However, this should be considered as a minimum number, since the postsynaptic targets were not reconstructed over sufficient length, and only those symmetrical synapses were noted which contacted the postsynaptic profile in the same sections as the thalamic terminal.

DISCUSSION

Origin and arborisation pattern of thalamocortical axons

Direct evidence that the axons described here, as in earlier studies (Blasdel and Lund, '83; Florence and Casagrande, '87), originated from the magno- and parvicellular layers of the lateral geniculate nucleus (LGN) cannot be given. However, if taken together, their receptive field properties, laminae of termination, and the clustering of their terminal boutons are consistent only with their origin being the magno- and parvicellular layers of the LGN. Even in the small sample of the present study it is clear that there is considerable variability in the size and extent of the terminal arbors. One parvicellular axon (PA1) formed two clumps; the other (PA2) formed one clump. Both magnocellular axons formed clumps, but in one of them the two clumps fused; in the other the clumps were quite separate but differed in size. In general, the injected axons were more extensive and contained more boutons than those reported by Blasdel and Lund ('83). There may be several reasons for this, including intrinsic variability in the axonal morphology, methodological differences, and differences in the region of area 17 in which the injected axons arborized.

Fig. 12. Lamellar bodies (arrows), an organelle similar to the spine apparatus in structure, in GABA-negative dendritic shafts postsynaptic to either magnocellular or parvicellular afferents. The GABA-immunogold reaction is shown in **F** and **H** for dendritic shafts contacted by a magnocellular (b_{MA}) and a parvicellular terminal (b_{PA}), and their nonimmunostained neighbouring sections in E and G, respectively. The lamellar bodies were usually apposed to a mitochondrion, whereas their other sides were facing the thalamic synapse (**A–E, G**). GABA-positive boutons (asterisks) of unknown origin are also indicated in F and H as a control for the quality of immunostaining. Scales: A–H, 0.5 μm.

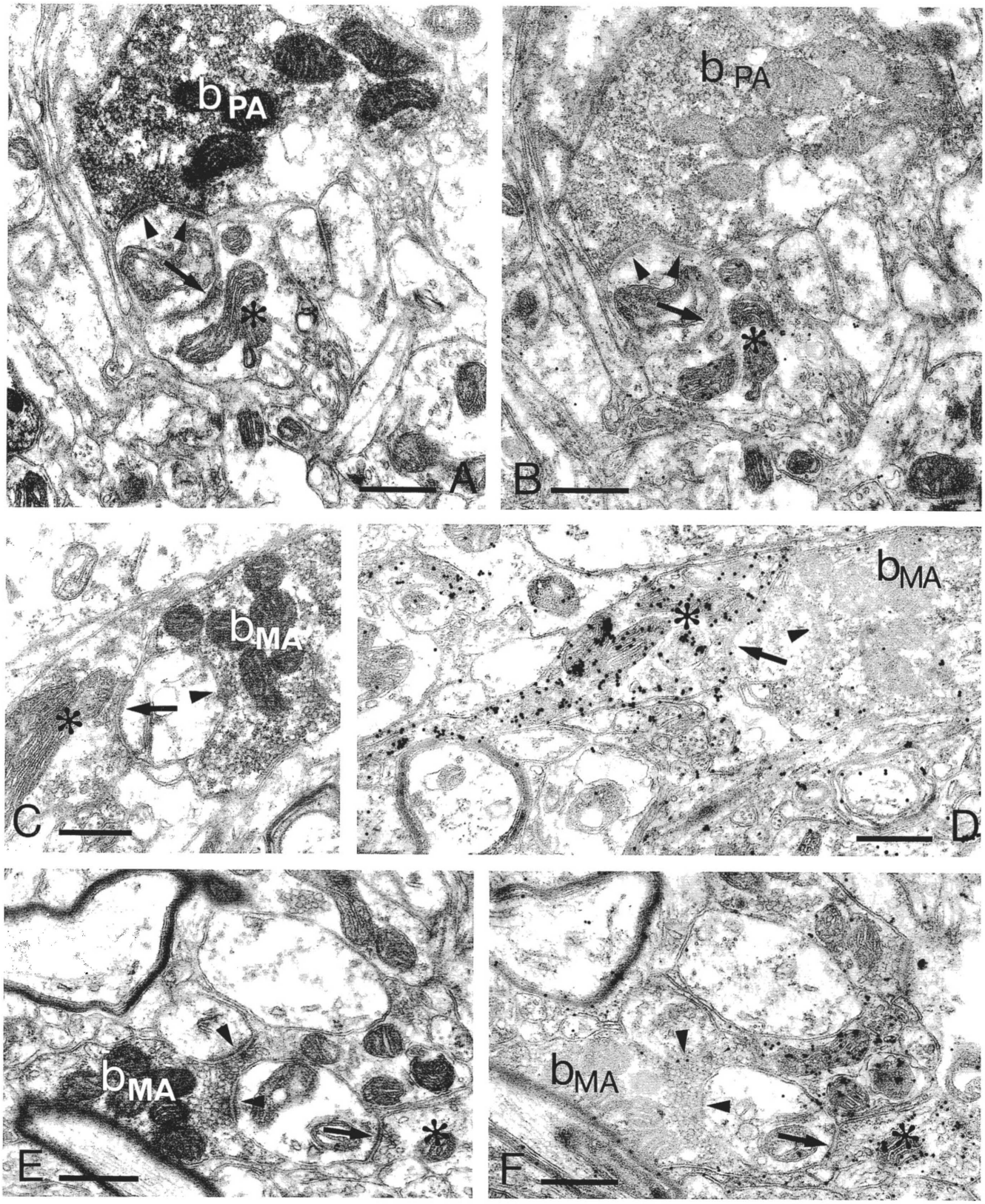

Fig. 13. A, B: Alternate sections of a parvicellular (b_{PA}) and magnocellular (b_{MA}) axon terminals in asymmetrical synaptic contact (arrowheads) with dendritic shafts (**A, B** and **E, F**) or a spine (**C, D**), which also receives a symmetrical synapse (arrow) from a GABA-immunoreactive bouton (asterisk). Sections in B, D, and F have been stained for GABA by the immunogold procedure; thus the accumulation of gold particles identifies the GABAergic structures (asterisk). The thalamic synapses are always asymmetrical (arrowheads), while the GABAergic synapses are symmetrical (arrows). Scales: A–F, 0.5 μm.

It was notable that for all the axons the dominant projection was to layer 4C. Layer 6 received only a tiny input by comparison. In this respect the axons in the monkey are similar to the X and Y axons of the LGN of the cat, where the dominant projection is also to layer 4 (LeVay and Gilbert, '76; Ferster and LeVay, '78; Gilbert and Wiesel, '79; Freund et al., '85a,b; Humphrey et al., '85). However, electrophysiological studies show that in both cat (Bullier and Henry, '79; Ferster and Lindstrom, '83; Martin and Whitteridge, '84) and monkey (Bullier and Henry, '80) the neurons in layer 6 are monosynaptically activated from the thalamus. The anatomical data from the present study and others (White and Hersch, '82; Blasdel and Lund, '83; Freund et al., '85b) suggest that this activation may well occur via the apical dendrites of layer 6 neurons as they pass through layer 4.

In layer 4C the extent of the individual axonal arborisations of intracellularly filled axons is greater than that of the dendritic spread of the recipient neurons. Thus both the parvicellular and the magnocellular axons will innervate many neurons. Blasdel and Fitzpatrick ('84) have calculated on the basis of similar data that 20–40 parvicellular afferents overlap at each point in layer 4Cβ. Our data suggest that this figure may be even higher. If dendritic spread is taken into consideration then each neuron in layer 4Cβ could potentially receive input from a hundred or more parvicellular thalamic neurons. Whether the degree of convergence is as high as this we have been unable to establish, but that some convergence does occur is suggested by the fact that a large proportion of layer 4Cβ neurons are not strongly selective for wavelength (Bullier and Henry, '80; Blasdel and Fitzpatrick, '84; Livingstone and Hubel, '84), whereas the majority of parvicellular layer neurons in the LGN are wavelength tuned (Wiesel and Hubel, '66; DeValois, '73; Dreher et al., '76; Kruger, '77).

Thalamocortical axons and retinotopic precision

There are relatively fewer LGN neurons available to innervate the cortical representation of the central visual field than to innervate the peripheral representation in the calcarine sulcus (Connolly and van Essen, '84). Thus, if the same coverage factor (axonal arbors covering a point in cortex) is to be maintained throughout the striate cortex, the axonal arbors in the foveal representation will have to be larger than those located in the periphery. This would not be compatible with the mapping precision if the grain of the map were determined by the size of the afferent arbor. As yet there are too few complete axons available, and there is too much variability in size even at a single eccentricity for reasonable comparisons to be made.

It has been suggested that "intrinsic processing" might serve to sharpen the topographical precision of the map in layer 4C (Blasdel and Lund, '83; Blasdel and Fitzpatrick, '84). The physiological data that led to this suggestion come mainly from extracellular recordings from postsynaptic neurons. These measurements of the size of the receptive fields and their ordering would only reflect the afferent organization precisely if one or a few afferents from the LGN provided the excitatory drive to a single neuron. The alternative view, that the receptive field is formed by the contribution of many afferents, allows the possibility for subthreshold excitation to extend beyond the borders of the field mapped extracellularly. In this view, the extracellular field would not give a precise estimate of the afferent distribution. Instead, it could produce a less precise mapping of the afferents. The extracellular receptive field would represent only the peak statistical effect of a large number of afferents, with each afferent making only a minor contribution. The contribution of the periphery may not be visible in the extracellular record but would appear as a subthreshold depolarization in an intracellular record. Such subthreshold events have been seen in cat visual cortex (Benevento et al., '72), but similar experiments have yet to be performed in the monkey. Inhibitory connections—involved in "intrinsic processing" mechanisms—may be important here in ensuring that only the peak response reaches threshold for spike discharge. This hypothesis may explain that both in the visual (Tsumoto et al., '79) and in the somatosensory cortex (Dykes et al., '84) the size of receptive fields increases when GABAergic inhibition is antagonised by bicuculline. This inhibition would not have to be tonic but could be activated by the incoming volley.

The clumps of terminals separated by unoccupied spaces can disrupt the retinotopic map, but as shown by Blasdel and Lund ('83) for one axon, the most likely reason for the patchy distribution is that individual axons can contribute to several ocular dominance columns. The contribution to several ocular dominance columns by axons which have their cortical position at the edge of an ocular dominance slab will ensure the continuity of the map for each eye separately. This is probably true for both the magnocellular and the parvicellular afferents. Furthermore, ordering within the ocular dominance slabs as detected by extracellular recording (Blasdel and Fitzpatrick, '84) is also possible because at least in one dimension the axonal arbors in 4Cβ are smaller than the ocular dominance columns.

Parvicellular and magnocellular axons contact a similar range of postsynaptic elements

The identity of the postsynaptic targets has been established in serial sections. Dendritic shafts and spines were distinguished on the basis of the presence of mitochondria and microtubules in dendritic shafts and their absence from dendritic spines. Using these criteria and serial reconstruction, we found a higher proportion of postsynaptic dendritic shafts and fewer dendritic spines than in earlier reports in the macaque (Garey and Powell, '71; Winfield et al., '82; Winfield and Powell, '83) and squirrel monkey (Tigges and Tigges, '79). In a preliminary study we have reconstructed the heads of 36 spines of five Golgi-impregnated spiny stellate cells in area 17 of the macaque monkey, and none of these contained mitochondria. Furthermore, to our knowledge, no identified spines with mitochondria have yet been published. The postsynaptic profiles containing both mitochondria and lamellar bodies must be therefore dendritic shafts.

Both the MA and PA afferents establish more synapses on dendritic shafts (30–40%) and fewer on dendritic spines than either the X- or Y-type geniculocortical axons in the cat (Freund et al., '85a). This correlates well with the observation that spiny stellate cells in the monkey have fewer spines than those in the cat (Lund et al., '79; Peters and Regidor, '81; Mates and Lund, '83a,b,c; Saint Maire and Peters, '85). The functional correlates of these differences are not known, but the biophysical properties of spiny stellate cells are likely to be different in the cat and monkey. Pyramidal cells with densely spiny dendrites were also a

major target for geniculocortical axons in the cat (Hornung and Garey, '81; Freund et al., '85b). In the monkey pyramidal cells are absent from layer 4C, and many of the apical dendrites passing through from infragranular layers have reduced density of spines in layer 4C. Thus the available spine population is probably smaller in the monkey.

The distribution of postsynaptic elements of the PA and MA afferents is similar; one MA and one PA axon established more synapses on dendritic shafts and less on dendritic spines than the other two axons. The proportion of GABAergic target elements, including all postsynaptic cell bodies and some of the dendritic shafts, is also similar. This striking similarity in the choice of basic types of postsynaptic elements suggests that the two parallel streams use a similar strategy at the first stage of information transfer to cortical circuits; i.e., the same basic types of neurons with similar relative frequencies are used as monosynaptic targets.

Selective presence of lamellar bodies in non-GABAergic dendrites

Lamellar bodies were found only in GABA-negative dendritic shafts; thus they can serve as ultrastructural markers of spiny, non-GABAergic dendrites. The possible role of the lamellar body is not known, but its structural similarity to the spine apparatus suggests that it may be involved in similar functions. The spine apparatus in Purkinje cell spines in the cerebellum was recently shown to accumulate calcium from the extracellular space, and the amount of calcium taken up is dependent on activation of parallel-fibre synapses terminating on these spines (Andrews et al., '88). We suggest that lamellar bodies in dendritic shafts of spiny cells may function in the same way, i.e., accumulate calcium which invades the dendrites via the synaptically activated calcium channels. Lamellar bodies preferentially occur at thalamic synapses since they were frequently found when studying targets of thalamocortical boutons but were rarely seen in random serial sections through dendrites of spiny cells. Their position within the dendrite (e.g., between the thalamic synapse and a mitochondrion, with a larger or swollen saccule facing the thalamic synapse) suggests that the site of entry of calcium may be at the thalamic synapse. Lamellar bodies have not been reported in the cat, even when dendritic shafts postsynaptic to thalamocortical afferents were studied (Freund et al., '85a, b). In the cat, in contrast to the monkey, the overwhelming majority (over 90%) of thalamic synapses to spiny cells terminated on dendritic spines (Freund et al., '85a,b), most of which contain a spine apparatus. In the monkey the GABAergic neurons, although they receive substantial thalamic inputs, have never been found to contain lamellar bodies. If our hypothesis for the role of lamellar bodies was correct the GABAergic neurons would have to use other means of buffering intracellular calcium, e.g., by calcium-binding proteins, one of which, parvalbumin, was shown to be selectively present in GABAergic neurons in the neocortex (Celio, '86).

Receptive field properties and activation of GABAergic interneurons

An aspect of cortical organization which could involve GABAergic inhibition is orientation selectivity (for review see Sillito, '84; Martin, '88). If inhibition plays a major role, then the relationship of the afferents to inhibitory interneurons will be important. In the cat cortex there is evidence that inhibition, involved in shaping of receptive field properties, is mediated by GABAergic interneurons (see Sillito, '84). Inhibitory circuitry in the monkey is likely to follow a similar design given that at least 15–20% of layer 4 cells contain GABA (Fitzpatrick et al., '87; Hendry et al., '87), and the neuronal types are similar (Szentágothai, '73; Lund et al., '79; Kisvarday et al., '85, '86; Lund, '87). However, if the elaboration of orientation selectivity was a major role for GABAergic neurons in layer 4C, one would expect differences between the magnocellular sublayer, where oriented cells predominate, and the parvicellular sublayer where most cells have nonoriented receptive fields (see above). We have examined two aspects of the GABAergic neuronal circuitry in layer 4C. Firstly, we compared the innervation of the GABAergic neurons in layers 4Cα and 4Cβ. There was no difference between the two afferent types in the proportion of GABAergic neurons contacted, nor in their target sites. Secondly, we examined the relationship between the thalamic input and GABAergic input to the same neuron. Here we found that GABAergic synapses were frequently located in close proximity to both parvi- and magnocellular axonal synapses. The implication is that the inhibitory synapse is located in this position so that it can effectively control the excitatory current with a degree of selectivity for the particular thalamic synapse. However, again there appeared to be no clear difference between the magno- and parvicellular axons in this respect. Thus, we found nothing in these aspects of the GABAergic circuitry that explained the difference in the orientation tuning of layer 4Cα vs. 4Cβ neurons (Bullier and Henry, '80; Blasdel and Fitzpatrick, '84; Hawken and Parker, '84; Livingstone and Hubel, '84).

An alternative explanation of the difference in the orientation tuning of layer 4Cα neurons compared to those of 4Cβ may lie in the tangential organization of cortical connections. These connection are much more extensive in the α than in β subdivision (Fitzpatrick et al., '85) for the thalamic afferents (Blasdel and Lund, '83; present study), for the excitatory spiny stellate axons within layer 4C (Kisvarday et al., '89), and for the inhibitory basket cell axons (Lund, '87). The longer lateral connections may allow the elongation of cortical receptive fields from geniculate cell fields, as originally proposed (Hubel and Wiesel, '62), boosted by long-range intracortical excitatory connections and sharpened by long-range inhibition. The more extensive lateral connections of the spiny stellate axons may support more boutons; thus for layer 4Cα cells a larger proportion of their synapses may come from intracortical sources.

The proportion of thalamic synapses on spiny stellate cells is not known in the monkey. The only study that addressed this question, using a degeneration method in the monkey, estimated that even in 4Cβ, only a few percent of synapses come from the lateral geniculate nucleus for any single neuron (Kisvarday et al., '86). With the same method the proportion of thalamocortical synapses on a spiny stellate cell in the mouse somatosensory cortex was estimated to be around 13% (White and Rock, '80). These low figures indicate that intracortical connections provide the majority of synapses for layer 4 neurons. The most obvious source is from other spiny stellate cells which form type 1 synapses in layer 4C (Saint Maire and Peters, '85; Kisvarday et al., '86) and by their sheer number provide a substantial contribution to their own layer.

The types of GABA-containing neurons innervated by PA or MA afferents in this study cannot be directly established even from serial electron microscopic sections. There is a

large variety of cells with smooth dendrites in layer 4C (Lund, '87), any one of which could be a target of the geniculate afferents. The most frequent type of all layer 4C GABAergic cells appears to be the clutch cell (clewed cell of Valverde, '71; Kisvarday et al., '86; β-1/α-1 type of Lund, '87) with axon arborisations matching those of the parvicellular thalamic afferents. The diameter of its terminal field in layer 4Cβ is about 100–150 μm and gives a small projection to layer 6 (Lund, '73, '87; Kisvarday et al., '86), as do PA afferents. Clutch cells have been shown to be GABAergic and to establish symmetrical synaptic contacts mainly with dendritic shafts and spines of spiny stellate cells (Kisvarday et al., '86). This cell type is the most likely candidate for the origin of the GABAergic boutons making symmetrical synapses with thin dendritic shafts and spines in close association with the thalamic synapses (Fig. 13).

It may be speculated that if the GABAergic neurons were monosynaptically driven by inputs from the LGN, as our results suggest, they would produce a feed-forward inhibition, which may be able to interact selectively with the thalamic input in the dendritic region. The function of such a feed-forward inhibition may be to control the influence of subthreshold excitatory inputs under certain conditions. Most cortical cells, including those in layer 4C, have antagonistic subregions in their receptive fields. Both in the monkey (Schiller, '82) and in the cat (see Sillito, '84) inhibitory interactions have been demonstrated between the subregions. As suggested earlier (Kisvarday et al., '86) the strengthening of the antagonism between subregions may be a role for some cortical inhibitory cells in all layers, and it could be of particular importance in layer 4C, where the receptive fields of different geniculate cells are combined for the first time.

ACKNOWLEDGMENTS

The authors are grateful to Mrs. K. Boczko, Mrs. K. Somogyi, Ms. J. Ellis, Mr. J. Anderson, and Mr. J.D. Roberts for excellent technical assistance. We thank Mr. J.D. Roberts and Dr. J. Somogyi for computer reconstructions and Prof. M.J. Friedlander, Centre for Neuroscience, University of Alabama, Birmingham, for facilities. The study was supported by the Medical Research Council UK and the Hungarian Academy of Sciences. T.F.F. was supported by the FIDIA Ischemia Research Fund, and I.S. was a scholar of the Herbert von Karajan Neuroscience Research Trust.

LITERATURE CITED

Adams, J.C. (1981) Heavy metal intensification of DAB-based HRP reaction product. J. Histochem. Cytochem. *29*:775.

Andrews, S.B., R.D. Leapman, D.M.D. Landis, and T.S. Reese (1988) Activity-dependent accumulation of calcium in Purkinje cell dendritic spines. Proc. Natl. Acad. Sci. USA *85*:1682–1685.

Benevento, L.A., O.D. Creutzfeldt, and U. Kuhnt (1972) Significance of intracortical inhibition in the visual cortex. Nature (New Biol.) *238*:124–126.

Blasdel, G.G., and D. Fitzpatrick (1984) Physiological organization of layer 4 in macaque striate cortex. J. Neurosci. *4*:880–895.

Blasdel, G.G., and J.S. Lund (1983) Termination of afferent axons in macaque striate cortex. J. Neurosci. *3*:1389–1413.

Bullier, J., and G.H. Henry (1979) Laminar distribution of first-order neurons and afferent terminals in cat striate cortex. J. Neurophysiol. *42*:1271–1281.

Bullier, J., and G.H. Henry (1980) Ordinal position and afferent input of neurons in monkey striate cortex. J. Comp. Neurol. *193*:913–935.

Celio, M.R. (1986) Parvalbumin in most γ-aminobutyric acid-containing neurons of the rat cerebral cortex. Science *231*:995–997.

Connolly, M., and D. van Essen (1984) The representation of the visual field in parvicellular and magnocellular layers of the lateral geniculate nucleus in the macaque monkey. J. Comp. Neurol. *226*:544–564.

DeValois, R.L. (1979) Central mechanisms of color visions. In R. Jung (ed): Handbook of Sensory Physiology. New York: Springer, pp. 209–253.

DeYoe, E.A., and D.C. van Essen (1988) Concurrent processing streams in monkey visual cortex. TINS *11*:219–226.

Dow, B.M. (1974) Functional classes of cells and their laminar distribution in monkey visual cortex. J. Neurophysiol. *37*:927–946.

Dreher, B., Y. Fukada, and R.W. Rodieck (1976) Identification, classification and anatomical segregation of cells with X-like and Y-like properties in the lateral geniculate nucleus of the old-world primates. J. Physiol. (Lond.) *258*:433–452.

Dykes, R.W., P. Landry, R. Metherate, and T.P. Hicks (1984) Functional role of GABA in cat primary somatosensory cortex: Shaping receptive fields of cortical neurons. J. Neurophysiol. *52*:1066–1093.

Ferster, D., and S. LeVay (1978) The axonal arborization of lateral geniculate neurons in the striate cortex of the cat. J. Comp. Neurol. *182*:923–944.

Ferster, D., and S. Lindstrom (1983) An intracellular analysis of geniculo-cortical connectivity in area 17 of the cat. J. Physiol. (Lond.) *342*:181–215.

Fitzpatrick, D., J.S. Lund, and G.G. Blasdel (1985) Intrinsic connections of macaque striate cortex: Afferent and efferent connections of lamina 4C. J. Neurosci. *5*:3329–3349.

Fitzpatrick, D., J.S. Lund, D.E. Schmechel, and A.C. Towles (1987) Distribution of GABAergic neurons and axon terminals in the Macaque striate cortex. J. Comp. Neurol. *264*:73–91.

Florence, S.L., and V.A. Casagrande (1987) Organization of individual afferent axons in layer IV of striate cortex in a primate. J. Neurosci. *7*:3850–3868.

Freund, T.F., K.A.C. Martin, A.D. Smith, and P. Somogyi (1983) Glutamate decarboxylase-immunoreactive terminals of Golgi-impregnated axo-axonic cells and of presumed basket cells in synaptic contact with pyramidol neurons of the cat's visual cortex. J. Comp. Neurol. 221:263–278.

Freund, T.F., K.A.C. Martin, P. Somogyi, and D. Whitteridge (1985a) Innervation of cat visual areas 17 and 18 by physiologically identified X- and Y-type thalamic afferents. II. Identification of postsynaptic targets by GABA immunocytochemistry and Golgi impregnation. J. Comp. Neurol. *242*:275–291.

Freund, T.F., K.A.C. Martin, and D. Whitteridge (1985b) Innervation of cat visual areas 17 and 18 by physiologically identified X- and Y-type thalamic afferents. I. Arborisation patterns and quantitative distribution of postsynaptic elements. J. Comp. Neurol. *242*:263–274.

Garey, L.J., and T.P.S. Powell (1971) An experimental study of the termination of the lateral geniculo-cortical pathway in the cat and monkey. Proc. R. Soc. Lond. [Biol.] *179*:41–63.

Gilbert, C.D., and T.N. Wiesel (1979) Morphology and intracortical projections of functionally characterised neurones in the cat visual cortex. Nature *280*:120–125.

Hanker, J.S., P.E. Yates, C.B. Metz, and A. Rustioni (1977) A new specific, sensitive and non-carcinogenic reagent for the demonstration of horseradish peroxidase. Histochem. J. *9*:789–792.

Hawken, M.J., and A.J. Parker (1984) Contrast sensitivity and orientation selectivity in lamina IV of the striate cortex of old world monkeys. Exp. Brain Res. *54*:367–372.

Hendrickson, A.E., J.R. Wilson, and M.P. Ogren (1978) The neuroanatomical organization of pathways between the dorsal lateral geniculate nucleus and visual cortex in old world and new world primates. J. Comp. Neurol. *182*:123–136.

Hendrickson, A.E., S.P. Hunt, and F.-Y. Wu (1981) Immunocytochemical localisation of glutamic acid decarboxylase in monkey striate cortex. Nature 262:605–607.

Hendry, S.H.C., H.D. Schwark, E.G. Jones, and J. Yan (1987) Numbers and proportions of GABA-immunoreactive neurons in different areas of monkey cerebral cortex. J. Neurosci. *7*:1503–1519.

Hodgson, A.J., B. Penke, A. Erdei, I.W. Chubb, and P. Somogyi (1985) Antiserum to γ-aminobutyric acid. I. Production and characterisation using a new model system. J. Histochem. Cytochem. *33*:229–239.

Hornung, J.P., and L.J. Garey (1981) The thalamic projection to cat visual cortex: Ultrastructure of neurons identified by Golgi impregnation or retrograde horseradish peroxidase transport. Neuroscience *6*:1053–1068.

Hubel, D.H., and T.N. Wiesel (1962) Receptive fields, binocular interaction and functional architecture in the cat's visual cortex. J. Physiol. (Lond.) *160*:106–154.

Hubel, D.H., and T.N. Wiesel (1968) Receptive fields and functional architecture of monkey striate cortex. J. Physiol. (Lond.) *195*:215–243.

Hubel, D.H., and T.N. Wiesel (1972) Laminar and columnar distribution of geniculo-cortical fibers in the macaque monkey. J. Comp. Neurol. *146*:421–450.

Hubel, D.H., and T.N. Wiesel (1977) Functional architecture of macaque monkey visual cortex. Proc. R. Soc. Lond. [Biol.] *198*:1–59.

Humphrey, A.L., M. Sur, D.J. Uhlrich, and S.M. Sherman (1985) Projection patterns of individual x- and y-cell axons from the lateral geniculate nucleus to cortical area 17 in the cat. J. Comp. Neurol. *233*:159–189.

Kennedy, H., K.A.C. Martin, G.A. Orban, and D. Whitteridge (1985) Receptive field properties of neurons in visual area 1 and visual area 2 of the baboon. Neuroscience *14*:405–415.

Kisvarday, Z.F., K.A.C. Martin, D. Whitteridge, and P. Somogyi (1985) Synaptic connections of intracellularly filled clutch cells: A type of small basket cell in the visual cortex of the cat. J. Comp. Neurol. *241*:111–137.

Kisvarday, Z.F., A. Cowey, A.D. Smith, and P. Somogyi (1989) Interlaminar and lateral excitatory amino acid connections in the striate cortex of monkey. J. Neurosci. (in press).

Kisvarday, Z.F., A. Cowey, and P. Somogyi (1986) Synaptic relationships of a type of GABA-immunoreactive neuron (clutch cell), spiny stellate cells and lateral geniculate nucleus afferents in layer IVC of the monkey striate cortex. Neuroscience *19*:741–761.

Kruger, J. (1977) Stimulus dependent colour specificity of monkey lateral geniculate neurons. Exp. Brain Res. *30*:297–311.

LeVay, S., and C.D. Gilbert (1976) Laminar patterns of geniculocortical projection in the cat. Brain Res. *113*:1–19.

Livingstone, M.S., and D.H. Hubel (1984) Anatomy and physiology of a colour system in the primate visual cortex. J. Neurosci. *4*:309–356.

Livingstone, M.S., and D.H. Hubel (1987) Psychophysical evidence for separate channels for the perception of form, color, movement, and depth. J. Neurosci. *7*:3416–3468.

Lund, J.S. (1973) Organisation of neurons in the visual cortex, area 17, of the monkey (Macaca mulatta). J. Comp. Neurol. *147*:455–496.

Lund, J.S. (1987) Local circuit neurons of macaque monkey striate cortex: I. Neurons of laminae 4C and 5A. J. Comp. Neurol. *257*:60–92.

Lund, J.S., and R. Boothe (1975) Interlaminar connections and pyramidal neuron organization in the visual cortex, area 17, of the macaque monkey. J. Comp. Neurol. *159*:305–334.

Lund, J.S., G.H. Henry, C.L. MacQueen, and A.R. Harvey (1979) Anatomical organization of the primary visual cortex (area 17) of the cat. A comparison with area 17 of the macaque monkey. J. Comp. Neurol. *184*:599–618.

Martin, K.A.C. (1988) From single cells to simple circuits in the cerebral cortex. J. Exp. Physiol. *73*:637–702.

Martin, K.A.C., and D. Whitteridge (1984) Form, function, and in intracortical projections of spiny neurons in the striate visual cortex of the cat. J. Physiol. (Lond.) *353*:463–504.

Mates, S.L., and J.S. Lund (1983a) Developmental changes in the relationship between type 2 synapses and spiny neurons in the monkey visual cortex. J. Comp. Neurol. *221*:98–105.

Mates, S.L., and J.S. Lund (1983b) Spine formation and maturation of type 1 synapses on spiny stellate neurons in primate visual cortex. J. Comp. Neurol. *221*:91–97.

Mates, S.L., and J.S. Lund (1983c) Neuronal composition and development in lamina 4C of monkey striate cortex. J. Comp. Neurol. *221*:60–90.

Peters, A., and J. Regidor (1981) A reassessment of the forms of nonpyrmidal neurons in area 17 of cat visual cortex. J. Comp. Neurol. *203*:685–716.

Ramón y Cajal, S. (1899) Estudios sobre la corteza cerebral humana. Corteza visual. Rev. Trim. Microgr. *4*:1–63.

Reynolds, E.S. (1963) The use of lead citrate at high pH as an electron opaque stain in electron microscopy. J. Cell Biol. *17*:208–212.

Saint Marie, R.L., and A. Peters (1985) The morphology and synaptic connections of spiny stellate neurons in monkey visual cortex (area 17): A Golgi-electron microscopic study. J. Comp. Neurol. *233*:213–235.

Schiller, P.H. (1982) Central connections of the retinal ON and OFF pathways. Nature *297*:580–583.

Shapley, R., E. Kaplan, and R. Soodak (1981) Spatial summation and contrast sensitivity of X and Y cells in the lateral geniculate nucleus of the macaque. Nature *292*:543–545.

Sillito, A.M. (1984) Functional considerations of the operation of GABAergic inhibitory processes in the visual cortex. In E.G. Jones and A. Peters (eds): Cerebral Cortex. Functional properties of Cortical Cells. New York: Plenum Press, pp. 97–117.

Somogyi, P., and A.J. Hodgson (1985) Antiserum to γ-aminobutyric acid. III. Demonstration of GABA in Golgi-impregnated neurons and in conventional electron microscopic sections of cat striate cortex. J. Histochem. Cytochem. *33*:249–257.

Somogyi, P., and I. Soltesz (1986) Immunogold demonstration of GABA in synaptic terminals of intracellularly recorded, horseradish peroxidase-filled basket cells and clutch cells in the cat's visual cortex. Neuroscience *19*:1051–1065.

Somogyi, P., A.J. Hodgson, and A.D. Smith (1979) An approach to tracing neuron networks in the cerebral cortex and basal ganglia. Combination of Golgi-staining, retrograde transport of horseradish peroxidase and anterograde degeneration of synaptic boutons in the same material. Neuroscience *4*:1805–1852.

Szentágothai, J. (1975) The 'module-concept' in cerebral cortex architecture. Brain Res. *95*:475–496.

Szentágothai, J. (1973) Synaptology of the visual cortex. In R. Jung (ed): Handbook of Sensory Physiology. Berlin: Springer-Verlag, pp. 269–324.

Tigges, M., and J. Tigges (1979) Types of degenerating geniculocortical axon terminals and their contribution to layer IV of area 17 in the squirrel monkey (Saimiri). Cell Tissue Res. *196*:471–486.

Tsumoto, T., W. Eckart, and O.D. Creutzfeldt (1979) Modification of orientation sensitivity of cat visual cortex neurons by removal of GABA-mediated inhibition. Exp. Brain Res. *34*:351–363.

Valverde, F. (1971) Short axon neuronal subsystems in the visual cortex of the monkey. Int. J. Neurosci. *1*:181–197.

White, E.L., and S.M. Hersch (1982) A quantitative study of thalamocortical and other synapses involving the apical dendrites of corticothalamic projection cells in mouse SmI cortex. J. Neurocytol. *11*:137–157.

White, E.L., and M.P. Rock (1980) Three-dimensional aspects and synaptic relationships of a Golgi-impregnated spiny stellate cell reconstructed from serial thin sections. J. Neurocytol. *9*:615–636.

Wiesel, T.N., and D.H. Hubel (1966) Spatial and chromatic interactions in the lateral geniculate body of the rhesus monkey. J. Neurophysiol. *29*:1115–1156.

Winfield, D.A., and T.P.S. Powell (1983) Laminar cell counts and geniculocortical boutons in area 17 of cat and monkey. Brain Res. *277*:223–229.

Winfield, D.A., M. Rivera-Dominguez, and T.P.S. Powell (1982) The termination of geniculocortical fibres in area 17 of the visual cortex in the macaque monkey. Brain Res. *231*:19–32.

Zeki, S., and S. Shipp (1988) The functional logic of cortical connections. Nature *335*:311–317.

Zsuppan, F. (1984) A new approach to merging neuronal tree segments traced from serial sections. J. Neurosci. Methods *10*:199–204.